

1 **Ab-initio dynamics of Gas-phase and Aqueous-phase Hydrolysis**  
2 **of Adenosine Triphosphate**

3 Raghav Saxena,<sup>1</sup> A. V. B. K. Sai Phani Kumar,<sup>1</sup> Raghvendra Singh,<sup>1</sup> and Vishal Agarwal<sup>1</sup>

4 *<sup>1</sup>Department of Chemical Engineering,*  
5 *Indian Institute of Technology Kanpur, Kanpur 208016, UP, India*

6 (Dated: October 26, 2020)

## Abstract

Adenosine triphosphate (ATP) hydrolysis is a well-known biological reaction which plays an important role in many biological processes. In this study, we have modelled the non-enzymatic hydrolysis of ATP in the gas-phase and the aqueous-phase by performing *ab initio* molecular dynamics simulations combined with an enhanced sampling technique. In the gas-phase, we studied hydrolysis of fully protonated ATP molecule and in the aqueous-phase, we studied hydrolysis of ATP coordinated with: a) *two*  $H^+$  ions (H-ATP), b)  $Mg^{2+}$  (Mg-ATP) and c)  $Ca^{2+}$  (Ca-ATP). We show that gas-phase ATP hydrolysis follows a two-step dissociative mechanism *via* a highly stable metaphosphate intermediate. The Adenine group of the ATP molecule plays a crucial role of a general base; temporarily accepting protons and, thus helping in the elimination-addition process. In the aqueous-phase hydrolysis of ATP, we find that the cage of solvent molecules increases the stability of the terminal phospho-anhydride bond through a well-known cage-effect. Further, in agreement with previous theoretical results, we find that the aqueous-phase hydrolysis happens with the help of nearby water molecules, which assumes the role of a base assisting in proton diffusion through Grotthuss mechanism. We obtained much lower free-energy barriers for the aqueous-phase hydrolysis of ATP coordinated with divalent ions ( $Mg^{2+}$  and  $Ca^{2+}$ ) compared to hydrolysis of ATP coordinated with only  $H^+$  ions, suggesting a clear catalytic effect of the divalent ions. The nature of the ions have an important effect on the mechanism of the reaction. We find a single-step dissociative-type mechanism for Mg-ATP, while we find a  $S_N-2$ -type concerted hydrolysis pathway for Ca-ATP.

## I. INTRODUCTION

Phosphoryl transfer reactions are ubiquitous in biological systems.<sup>1,2</sup> For example, signal transduction and basic metabolic pathways are hinged on the selective phosphoryl-transfer chemistry. Enzymatic hydrolysis of adenosine triphosphate (ATP) forms one such important class of biological reaction which provides energy for performing myriad of crucial functions inside our body, e.g., muscle contraction, chemical synthesis etc.<sup>3-6</sup> Enzymes help in selectively catalysing ATP hydrolysis by providing an alternate pathway of lower free-energy barrier. Since enzymes play such an important role in our body, it becomes imperative to study their rate-enhancing role. Such an understanding begins by first discerning the mech-

36 anistic details and barriers of an un-catalysed reaction—which forms the basis for further  
37 dissecting enzyme-catalysed reactions.

38 Over the last couple of decades, there has been intense debate about the mechanis-  
39 tic aspects of the non-enzymatic phosphate hydrolysis.<sup>2,7</sup> The discussions revolve around  
40 two extreme cases; namely the dissociative and the associative pathways. In the dissocia-  
41 tive mechanism, terminal phospho-anhydride bond breaks before the attack of nucleophilic  
42 water molecule. It involves the formation of a triangular planar metaphosphate-type in-  
43 termediate (or transition-state). Whereas, in the associative mechanism the attack of lytic  
44 water molecule takes place before breaking of the terminal phospho-anhydride bond, involv-  
45 ing the formation of a penta-coordinated trigonal bi-pyramidal phosphorus intermediate (or  
46 transition-state). Another interim reaction pathway is also highlighted, which is when the  
47 two events, i.e. breaking of the terminal phospho-anhydride bond and the attack of nucle-  
48 ophile, takes place simultaneously; and therefore, aptly known as the concerted mechanism.  
49 More elaborative description of the mechanistic details can be found elsewhere.<sup>2</sup>

50 Most studies support dissociative mechanism over associative mechanism.<sup>8–12</sup> For exam-  
51 ple, Akola and Jones (2003) studied hydrolysis of methyl triphosphate in aqueous solution  
52 and concluded that dissociative mechanism is more favourable than associative mechanism<sup>10</sup>.  
53 In contrast, a recent study by Wang et al. (2015) on ATP hydrolysis in aqueous solution  
54 suggested a mechanism in which reaction proceeds along concerted path from reactant state  
55 to transition state and along the associative path from transition state to product state<sup>13</sup>.  
56 Some studies, however, suggest that both mechanisms (dissociative and associative) are  
57 possible and the choice rather depends on the environment.<sup>12,14–16</sup> For example, Florián and  
58 Warshel (1998)<sup>14</sup> did a theoretical study on hydrolysis of methyl phosphate in an implicit  
59 aqueous-solution. The authors concluded that the barriers for associative and dissociative  
60 pathways are similar in solution and either of these can be operational depending on the  
61 electrostatic environment.

62 Beyond the classical classification of hydrolysis process into dissociative, associative and  
63 concerted reaction; ATP hydrolysis can also be classified as solvent-assisted or substrate-  
64 assisted mechanism.<sup>9</sup> As shown previously by Glaves et al. (2012), the nearby water  
65 molecules play an active role by transferring proton *via* proton shuttling along a chain  
66 of hydrogen-bonded network.<sup>9,12</sup> The hydrolysis reaction in which such a chain of water  
67 molecules are involved is known as solvent-assisted catalysis.<sup>12</sup> ATP also has a nitrogenous

68 head which can play an active role of a base and help in dynamic transfer of protons during  
69 the hydrolysis event.

70 A lot of theoretical studies already exists in literature elucidating the mechanism and  
71 barriers for phosphate hydrolysis.<sup>9-14,16-25</sup> However, majority of them are either done with  
72 simple model molecules like monophosphate esters, pyrophosphates<sup>14,16,22-25</sup> or done with  
73 truncated versions of ATP (for example, methyl triphosphate);<sup>9,10,12,16</sup> likely because of the  
74 computational intensive nature of these calculations. Very few have considered full ATP  
75 molecule in their study. In these studies either the head of ATP (adenosine part) is treated  
76 with molecular mechanics (MM)<sup>13</sup> or part of the aqueous system is treated with MM force-  
77 fields<sup>11</sup>.

78 In this study, we have modelled ATP hydrolysis in the gas-phase and the aqueous-phase  
79 by performing *ab initio* molecular dynamics simulations. We treat full ATP molecule at a  
80 quantum-mechanical level in the hope of capturing the possible role of the Adenosine group in  
81 ATP hydrolysis. Adenine group of the ATP head is a nitrogenous-base which can temporarily  
82 accept proton and help in the hydrolysis process. The role of the Adenosine group may  
83 become more relevant in the gas-phase or hydrophobic pockets of the enzyme.<sup>26,27</sup> Further,  
84 to elucidate the effect of nature of ions, we study hydrolysis of ATP by performing *three*  
85 simulations in the aqueous solution—1) ATP coordinated with H<sup>+</sup> ions, 2) ATP coordinated  
86 with Mg<sup>2+</sup> ion, and 3) ATP coordinated with Ca<sup>2+</sup> ion. We know of no previous study which  
87 has modelled the hydrolysis of Ca-ATP and H-ATP in aqueous solution. This will offer a  
88 comparison to the well studied Mg-ATP hydrolysis by several excellent studies before.<sup>10,12</sup>

89 We study gas-phase ATP hydrolysis for several reasons. First, it forms a vital comparison  
90 to understand the role of water. Second, some studies in the literature suggest that ATP's  
91 conformational state attached to the enzymatic protein is very different from that in the  
92 aqueous solution. For example, Kobayashi et al. (2013)<sup>28</sup> compared conformations of ATP  
93 in solution to that when complexed with a protein. They took a comprehensive list of ATP  
94 complexed to the protein from the protein data bank and computed several torsional angles  
95 to compare with the aqueous-phase ATP conformations. The authors concluded that ATP  
96 assumes a conformation on a protein that is rarely found in the aqueous solution. The  
97 most dominant conformer found in their study had a bent structure which suggests that  
98 gas-phase studies may be a more relevant comparison. Lastly, some studies have shown that  
99 in the enzymes' hydrophobic pockets, ATP hydrolysis takes place in the presence of one

100 water molecule. For example, Oldham et al. (2011)<sup>27</sup> determined the crystal structure of  
101 a bacterial ABC transporter, and Dawson et al. (2006)<sup>26</sup> determined crystal structures of  
102 the full-length wild-type maltose transporter. The studies demonstrate that such enzymatic  
103 pockets adopt a closed and compact conformation in which only one water molecule is allowed  
104 to react with the ATP. A recent study by Prieß et al. (2018)<sup>29</sup> modelled the mechanism  
105 of ATP hydrolysis in the ABC transporter by using hybrid QM/MM molecular dynamics  
106 simulations. The study also suggested that the two-water mechanism involves a significantly  
107 higher free energy barrier than the one-water mechanism and is unfavorable. This suggests  
108 that one water gas-phase study is an appropriate reference environment for such enzymatic  
109 reactions.

110 Exploring reactive-events in ATP hydrolysis, even in the gas-phase, is a daunting com-  
111 putational task. One of the reason for this is that the un-catalysed phosphate hydrolysis  
112 has a huge free-energy barrier. And, therefore, a brute-force *ab initio* molecular dynamics  
113 (AIMD) simulation fails to capture the reactive-event because of the time-scale problem.<sup>30</sup>  
114 The problem can be addressed by several available accelerated MD methods,<sup>31–35</sup> each hav-  
115 ing its own distinct advantage. We perform our studies using the Metadynamics method<sup>35</sup>  
116 which enhances the probability of the hydrolysis event by slowly adding repulsive poten-  
117 tials along certain collective variables defined in such a way to encompass the possibility of  
118 associative, dissociative and concerted reaction pathways.

119 The remainder of this article is organized as follows: in section 2 we briefly describe the  
120 methods used to generate initial ATP conformer in the gas-phase and aqueous-phase; we  
121 also offer computational details on *ab-initio* MD simulations and metadynamics. In section  
122 3, we give results and discussion on ATP hydrolysis in the gas-phase and the aqueous-phase  
123 elucidating the role of water and ions. Finally, in section 4, we offer concluding remarks.

## 124 II. METHODOLOGY

### 125 A. System Setup

126 Adenosine triphosphate (ATP) consists of three main components: the adenine ring, the  
127 ribose ring, and the triphosphate as shown in Figure 1. We denote the terminal phosphorous  
128 on the triphosphate as ‘ $P_\gamma$ ’ and the hydroxyl oxygen on this phosphorous as ‘ $O_{\gamma s}$ ’. We refer

129 the reader to Figure 1 for the rest of the symbols. In what follows, we denote ‘H-ATP’  
130 to be the state of ATP when  $O_{\alpha s}$ ,  $O_{\beta s}$  and two  $O_{\gamma s}$  are coordinated with  $H^+$  ions; ‘Mg-  
131 ATP’ when  $O_{\gamma s}$  and  $O_{\beta s}$  are coordinated with  $Mg^{2+}$  ion; and ‘Ca-ATP’ when  $O_{\gamma s}$  and  $O_{\beta s}$   
132 are coordinated with  $Ca^{2+}$  ion. In our aqueous-phase simulations, *two* protons on the tri-  
133 phosphate tail leave the ATP molecule during equilibration runs and are solvated in the  
134 aqueous-phase, thus forming a divalent ion. This is in concordance with the experimental  
135 studies that ATP exists as a divalent ion at low pH values.<sup>36,37</sup> At higher pH value, ATP  
136 may exist as a trivalent or a tetravalent ion which may change the reaction mechanism and  
137 barriers.<sup>38,39</sup> We do not study the effect of pH in this work.

### 138 1. Gas-Phase

139 In the gas-phase, we only studied the hydrolysis of H-ATP. H-ATP can exist in large  
140 number of conformers in the gas-phase. We found over 800 conformers in the gas-phase  
141 by performing simulated-annealing molecular dynamics simulations using AMBER(GAFF)  
142 force-field<sup>40</sup> using Gabedit software package.<sup>41</sup> The structures (and the energies) were fur-  
143 ther refined by performing geometry optimization with PM6-DH2 method<sup>42</sup> in MOPAC7  
144 software package.<sup>43</sup> The computational expense limits the feasibility of studying hydrolysis  
145 mechanism for each of these conformers. Moreover, the conformers span over  $\sim 300$  kJ/mol  
146 and the probability of existence of high-energy conformers is almost zilch. Therefore, we  
147 extracted conformers whose relative energies lied within 30 kJ/mol compared to the lowest  
148 energy conformer (about *seven* conformers satisfied this criteria). These conformers were  
149 further optimized with Density functional theory calculations using B3LYP/6-31+g(d)<sup>44-48</sup>  
150 as the model chemistry. We show comparison of electronic energies of these *seven* con-  
151 formers relative to the lowest energy conformer in Figure S1 of Supplementary information.  
152 The lowest energy conformer (i.e. conformer 3 in Figure S1) was used for studying the gas-  
153 phase hydrolysis mechanism. The conformer has a bent structure which is stabilized by the  
154 intra-molecular hydrogen bonding between the Adenosine-head and the phosphate-tail. For  
155 comparison, we also studied hydrolysis mechanism of a conformer which has a more open  
156 structure. Another reason for studying this conformer was that the previous experimental  
157 studies indicate presence of an open conformer in the aqueous-phase.<sup>49</sup> We show snapshots  
158 of these two conformers in Figure S2 of Supplementary Information and compare several

159 dihedral angles of these conformers in Table S1.

160 Further, to generate an initial guess for H-ATP/water complex in the gas-phase, we  
161 performed geometry optimizations on several positions of water near the triphosphate tail.  
162 We found *six* reactant complexes as shown in the Supplementary Information (Figure S3).  
163 The most stable complex was used for *ab initio* molecular dynamics and metadynamics  
164 simulations.

## 165 2. Aqueous-Phase

166 The initial structure for ATP (coordinated with either  $H^+$ ,  $Mg^{2+}$  or  $Ca^{2+}$ ) in the aqueous-  
167 phase was generated by performing classical molecular dynamic simulations using GRO-  
168 MACS simulation package (version 2018).<sup>50,51</sup> We used SPC/E force-field<sup>52</sup> for the water  
169 potential and AMBER(GAFF) force-field<sup>40</sup> for the rest of the interactions. The force-field  
170 parameter file for GROMACS was generated using the Acyppe software.<sup>53</sup> Following steps  
171 were used for these simulations. a) ATP was solvated in a cubic box of 25 Å using subrou-  
172 tines in GROMACS, which added about 490 water molecules to the simulation box. b) NVT  
173 molecular dynamics simulations were performed for 100ps by keeping ATP fixed. This was  
174 done to remove any bad contacts which might have been obtained due to random insertion  
175 of water molecules. c) The whole system (without any positional restraints on ATP) was  
176 then subjected to NPT molecular dynamics simulations for 5 ns. d) The average box-size for  
177 the last 2 ns was used for further runs. The system was thermally equilibrated for another  
178 100 ps by performing NVT molecular dynamics simulations. The coordinates and velocities  
179 from this run were used as an initial guess for studying ATP hydrolysis in the aqueous-phase.

180 The initial velocities for classical molecular dynamic simulations were obtained from  
181 Maxwell-Boltzman distribution. A time-step of 1 fs was used. System temperature was  
182 maintained at 310K by using the Nosé–Hoover Chain thermostat.<sup>54</sup>

## 183 B. Simulation Details

184 We used CP2K (version 5.1) software package<sup>55</sup> for performing all our production *ab*  
185 *initio* calculations. For benchmarking purposes, we also used Gaussian16 software package.<sup>56</sup>  
186 Density functional theory calculations were performed as formulated by Kohn-Sham<sup>57–60</sup>

187 with PBE as the exchange-correlation functional.<sup>61</sup> We used an atom-centered Gaussian-  
188 type basis for wave-functions and plane wave basis for density (GPW)<sup>62</sup> *via* an efficient  
189 implementation in CP2K, namely Quickstep.<sup>63</sup> The core electrons were described by norm-  
190 conserving Goedecker, Teter, and Hutter (GTH) pseudo-potential.<sup>64,65</sup> The wave-functions  
191 for outer electrons were expanded by triple-zeta valence basis with two set of polarisation  
192 function (TZV2P)<sup>66</sup> for all the atoms except for Ca which was treated with double-zeta basis  
193 with one set of polarization function (DZVP).<sup>66</sup> An energy cutoff of 300Ry for the gas-phase  
194 and 380 Ry for the aqueous-phase simulations were used for an auxiliary plane wave basis  
195 set. The cutoffs were enough to converge the total energy to within 0.01 eV. *Six* electrons  
196 ( $[2s^2 2p^4]$ ) for O atoms, *five* electrons ( $[2s^2 2p^3]$ ) for N atoms, *five* electrons ( $[3s^2 3p^3]$ ) for P  
197 atoms, *ten* electrons ( $[2s^2 2p^6 3s^2]$ ) for Mg atoms, *four* electrons ( $[2s^2 2p^2]$ ) for C atoms, and  
198 *ten* electrons ( $[3s^2 3p^6 4s^2]$ ) for Ca atoms were treated explicitly. Dispersion corrections were  
199 taken into account by the Grimme’s D3 method.<sup>67</sup> Mulliken scheme was used to compute  
200 charges on atoms (or group of atoms).

201 We performed NVT *ab initio* molecular dynamics simulations based on Born-Oppenheimer  
202 approach. A time-step of 0.5 fs was used to numerically integrate the molecular dynamics  
203 equations. A cubic box of 30 Å size was used for the gas-phase simulations and a box of  
204 25 Å size was used for the aqueous-phase simulations. Periodic boundary conditions were  
205 applied in all the three directions. Nosé–Hoover Chain thermostat<sup>54</sup> was used to maintain  
206 the system temperature at 310 K, which is the average temperature of the human body.

207 The initial coordinates for the system to study ATP hydrolysis in gas-phase and aqueous-  
208 phase were obtained by a systematic procedure as outlined above (*vide supra*).

### 209 1. Metadynamics

210 The barriers associated with ATP hydrolysis in aqueous-phase are typically around 130  
211 kJ/mol, which are much larger than  $k_B T$  at 310 K. The reactive events are, therefore,  
212 thermally-activated uncorrelated events with time-scales much greater than vibrational  
213 times; and hence termed as rare-events. To put this into perspective, we consider a hy-  
214 drolysis barrier of  $E_{\text{act}} = 130$  kJ/mol. For a pre-exponential factor of  $10^{13}$  s<sup>-1</sup>, the average  
215 time spend by the ATP in the reactant basin is  $\sim 10^9$  s—which is much larger than the  
216 time-scales accessible by a brute-force *ab initio* molecular dynamics simulations.

217 We have, therefore, used metadynamics method<sup>35,68–70</sup> which slowly coaxes the system to  
 218 a reactive event by adding repulsive potentials along the path of certain collective variables  
 219 at regular intervals. The collective variables are chosen in such a way to describe the process  
 220 of interest. We detail below the choice of collective variables (*vide infra*).

221 We have used the extended Lagrangian implementation of metadynamics<sup>68</sup> in CP2K to  
 222 probe the reactive-events. In this scheme, the repulsive potentials are added along the  
 223 auxiliary variables (one for each collective variable) of mass,  $m_\alpha$ , which are coupled to real  
 224 collective variables through harmonic springs of force constant,  $k_\alpha$ .

225 Several functional forms for repulsive potentials has been suggested in literature. In this  
 226 work, we have used the  $n$ -dimensional Gaussian function, where  $n$  is the number of collective  
 227 variables. Since we have two collective variables, a *two*-dimensional Gaussian function acts  
 228 as the repulsive potential. The free-energy was reconstructed from the history-dependent  
 229 potential using the equation:

$$\begin{aligned}
 \Delta F(s_1, s_2) = - \lim_{t \rightarrow \infty} \int_0^t \sum_{i=1}^{d(t')} & \left[ w(t') \delta(t' - t_i) \exp \left( - \left( \frac{(s_1(\vec{R}) - s_1(\vec{R}(t')))^2}{2\sigma_1^2} \right. \right. \right. \\
 & \left. \left. \left. + \frac{(s_2(\vec{R}) - s_2(\vec{R}(t')))^2}{2\sigma_2^2} \right) \right) \right] dt' \tag{1}
 \end{aligned}$$

231 where  $s_1$  and  $s_2$  are the two collective variables.  $t_i$  is the simulation time at which the  $i^{th}$   
 232 Gaussian is added to the accumulating bias potential,  $w(t')$  is the height and  $\sigma$  is the width  
 233 of each Gaussian.

234 A constant Gaussian height of  $w = 1$  kcal/mol ( $\sim 1.5k_B T$ ) was used—which serves as the  
 235 natural error in our simulations. A Gaussian width of  $\sigma = 0.05$  for each collective variable  
 236 was used in this work.  $m_\alpha$  was set to 50 *amu* and  $k_\alpha$  was set to 2 *au* to adiabatically separate  
 237 the dynamics of real space variables from auxiliary variables. A Gaussian hill deposition  
 238 rate of 0.05 fs<sup>-1</sup> was chosen to avoid the problem of hill-surfing.<sup>71</sup> The parameters are  
 239 chosen after several benchmarking studies as detailed in our previous work;<sup>72</sup> and they are  
 240 similar to the ones used in the previous work on nucleoside triphosphate hydrolysis.<sup>12,73–75</sup>  
 241 In our previous work on cellulose (a biological molecule) pyrolysis,<sup>72</sup> we showed that by  
 242 using the recipe suggested by Ensing et al. 2005, we were able to converge the free-energy  
 243 barriers of gas-phase methyl-glucoside and cellobiose decomposition to within the gaussian

244 height. To go beyond that one would need to perform well-tempered metadynamics<sup>76</sup> which  
 245 is currently too computationally expensive for the size of the system used in this work. The  
 246 natural error of our metadynamics simulations, i.e. the gaussian height, will not effect the  
 247 qualitative comparisons we have presented in this work.

## 248 2. Collective Variables

249 In this study we have used coordination number type collective variables (CV). We used  
 250 P–O coordination number as the CV in the metadynamics simulation which is described by  
 251 the following functional form:

$$252 \text{CN [P - O]} = \sum_{j \in \text{O}} \frac{1 - (R_{PO_j}/R_{PO}^o)^6}{1 - (R_{PO_j}/R_{PO}^o)^{12}} \quad (2)$$

253 where  $R_{PO}^o$  is distance cut off parameter which characterizes the bond between P–O. We  
 254 chose a value of  $R_{PO}^o = 4.5 \text{ a.u. } (\sim 2.38 \text{ \AA})$ . The following two collective variables were em-  
 255 ployed in this study: (a) CV1: coordination number of terminal phosphorus  $P_\gamma$  with bridging  
 256 oxygen  $O_{\beta b}$  (see Figure 1 for symbols), and (b) CV2: coordination number of terminal phos-  
 257 phorus  $P_\gamma$  with two  $\gamma$  oxygens, i.e.  $O_{\gamma s}$  and water oxygens  $O_w$ . For aqueous-phase study all  
 258 the water oxygens were included in CV2. This choice ensures we are not biasing our reaction  
 259 to one particular water molecule. The two collective variables were chosen to capture all  
 260 the possible mechanisms of ATP hydrolysis; namely dissociative, associative and concerted.  
 261 The collective variables used are similar to the ones used in previous studies.<sup>12,73–75</sup> CV1  
 262 represents the breaking and reformation of bond between  $P_\gamma$  and  $O_{\beta b}$ , and CV2 represents  
 263 the attack of nucleophilic water molecule on terminal phosphorus. We included  $\gamma$  oxygens  
 264 into CV2 after several trial metadynamics runs. Our trial runs without  $\gamma$  oxygens in CV2  
 265 had proton transfer from water to  $\gamma$  oxygen. In the process,  $O_{\gamma s}$  is released as water and  $O_w$   
 266 takes place of  $O_{\gamma s}$  in the ATP molecule; making CV2 redundant for the reaction we want  
 267 to study.

### 268 III. RESULTS AND DISCUSSION

#### 269 A. Hydrolysis of H-ATP in the gas-phase

270 We begin by detailing the hydrolysis reaction of H-ATP in the gas-phase, where we  
271 studied the hydrolysis of H-ATP by a single water molecule. ‘H-ATP’ refers to the state of  
272 ATP where phosphate oxygens are coordinated with  $H^+$  ions. We refer the reader to Sec.  
273 II A for notational details. As mentioned earlier, gas-phase studies become important in the  
274 enzymatic pocket where the environment for ATP hydrolysis is hydrophobic. Secondly, it  
275 becomes an important comparison to understand the role of water on the ATP hydrolysis  
276 reaction.

277 The restricted free energy surface computed using Eqn.1 is shown in Figure 2a. From this  
278 free-energy surface, we obtain an overall free-energy barrier of 32.3 kcal/mol. The free-energy  
279 barrier for the first and the second step are 20.6 kcal/mol and 31.3 kcal/mol, respectively.  
280 The metadynamics simulations on the random configuration yielded similar overall barriers  
281 and reaction mechanism (see Figure S4 in Supplementary Information); therefore, we do not  
282 analyse it further in this manuscript.

283 We note here that PBE functional is known to give an error within 0.2 eV. Also, free  
284 energy barriers might be affected by the selection of collective variables; therefore, we put  
285 little emphasis on the magnitude of the barriers and focus on the qualitative findings and  
286 comparisons.

287 The restricted free-energy surface (see Figure 2a) shows several distinct features. The  
288 reactant (denoted as ‘Reac’), the intermediate (denoted as ‘Int’), and the product state  
289 (denoted as ‘Prod’) can be identified from the free-energy minimas. The two saddle-points on  
290 the free-energy surface are the probable transition-states (denoted as ‘TS1’ and ‘TS2’): TS1  
291 is the transition-state between the reactant and the intermediate; and TS2 is the transition-  
292 state between the intermediate and the product. The snapshots of these states are shown  
293 in Figure 4.

294 We also provide a movie of the gas-phase metadynamics trajectory in the Supplementary  
295 Information (see Figure S5). During the whole process, we observe dynamic rearrangement  
296 of the protons involving the Adenine group, water molecule, and the tri-phosphate group of  
297 the ATP molecule as detailed below (*vide infra*).

298 In order to better understand the mechanism, we monitored the evolution of collective  
299 variables, bond distances and angles along the metadynamics trajectory. The changes in  
300 CV1 and CV2 with metadynamics time are plotted in Figure 3. We refer the reader to  
301 Sec.IIB2 for details on CV1 and CV2. CV1 is the coordination number of the terminal  
302 phosphorus  $P_\gamma$  with the bridging oxygen  $O_{\beta b}$ . A value of CV1 near *one*, indicates a chemical  
303 bond between  $P_\gamma$  and  $O_{\beta b}$ ; whereas a value near *zero* represents breaking of the  $P_\gamma$ - $O_{\beta b}$   
304 chemical bond. CV2 is the coordination number of terminal phosphorus  $P_\gamma$  with two  $\gamma$   
305 oxygens and water oxygen  $O_w$ . The value of CV2 is  $\sim 3$  when water oxygen has formed a  
306 bond with  $P_\gamma$ ; otherwise it is  $\sim 2$ .

307 Figure 3 and the reaction trajectory (see Figure S5 in Supplementary Information) shows  
308 a clear preference for the dissociative mechanism in the gas-phase. The reaction proceeds  
309 by first breaking the terminal  $O_{\beta b}$ - $P_\gamma$  bond and then the water molecule attacking the  
310 metaphosphate. At  $\sim 8$  ps metadynamics time, CV1 goes from a value of  $\sim 0.8$  to  $\sim 0.05$ ;  
311 signifying  $P_\gamma$  breaking its bond with  $O_{\beta b}$  and forming metaphosphate. At  $\sim 14$  ps, water  
312 molecule attacks the metaphosphate and water oxygen ( $O_w$ ) attaches itself to  $P_\gamma$  to form  
313 orthophosphate. This is evident from the increase in the value of CV2 from  $\sim 1.8$  to  $\sim 2.8$ ,  
314 as shown in Figure 3. The reaction also involves dynamic rearrangement of protons, which  
315 is not captured with the chosen collective variables. However, the rearrangement of protons  
316 is clearly visible in the movie of the reactive event (see snapshots in Figure 4) and we detail  
317 this below by plotting a sum of certain coordination numbers during the metadynamics run.

318 It is customary to gauge the nature of the reaction mechanism (whether associative, dis-  
319 sociative or concerted) in ATP hydrolysis using the More O’Ferrall-Jencks (MOFJ) plot.<sup>77,78</sup>  
320 The two-dimensional plot shows correlation of  $O_{\beta b}$ - $P_\gamma$  distance with the  $P_\gamma$ - $O_w$  distance.  
321 Since these distances directly relates to CV1 and CV2, the restricted free-energy surface  
322 gives us direct correlation with the MOFJ plot. For completeness, we present MOFJ plot  
323 for the gas-phase hydrolysis of H-ATP in Figure 5a. The trajectory from the upper-left  
324 corner (reactant) to the lower-right corner (product) *via* the upper-right corner represents  
325 the dissociative pathway; whereas, the trajectory *via* the lower-left corner represents the  
326 associative pathway. The trajectory *via* the diagonal is the concerted pathway. From the  
327 MOFJ plot in Figure 5a, it is clear that the gas-phase hydrolysis of H-ATP proceeds through  
328 the dissociative mechanism supporting our previous discussions.

329 At  $\sim 8$  ps, the first reactive event happens when  $P_\gamma$  parts away from the bridging oxygen,

330  $O_{\beta b}$ . This is evident from the increase in the distance between  $P_{\gamma}$  and  $O_{\beta b}$  from  $\sim 1.6\text{\AA}$  to  
331 more than  $3\text{\AA}$  (see lower panel of Figure 6). Terminal phosphorus  $P_{\gamma}$  goes from tetrahe-  
332 dral geometry in reactant state to a planar geometry after terminal  $P_{\gamma}-O_{\beta b}$  bond breaks in  
333 the intermediate state to again tetrahedral geometry after the attack of nucleophilic water  
334 molecule in the product state. We show these transitions by plotting the sum of  $\angle O-P-O$   
335 ( $\angle\theta$ ) of the terminal  $PO_3$  entity during the metadynamics run in Figure 6. After the first re-  
336 active event, the  $PO_3$  moiety of the terminal phosphate changes its  $\angle\theta$  from  $\sim 340^\circ$  to  $\sim 360^\circ$   
337 indicating a change in geometry from tetrahedral to planar, and the formation of metaphos-  
338 phate. From  $\sim 8 ps$  to  $\sim 14 ps$ , metaphosphate is either present as metaphosphate ion or  
339 metaphosphoric acid due to dynamic arrangement of protons. At  $\sim 14 ps$ , metaphosphate  
340 (planar geometry) converts to orthophosphate (tetrahedral geometry) after water oxygen  
341 attaches itself to the phosphorous. This is evident from the decrease in  $\angle\theta$  from  $\sim 360^\circ$  to  
342  $340^\circ$  as shown in Figure 6.

343 Interestingly, metadynamics trajectory predicts presence of an intermediate with a highly  
344 stabilized metaphosphate ion (only  $\sim 1$  kcal/mol higher in free-energy than the reactant  
345 configuration). Since, free-energy includes contributions from entropy; therefore, we also  
346 extracted coordinates of Reac (at  $0ps$ ), Int (at  $\sim 9.75 ps$ ) and Prod (at  $\sim 19.44ps$ ) and sub-  
347 jected them to geometry optimization. We plot electronic energies of Reac, Int, and Prod  
348 along with their optimized structures in Figure 7. Indeed, we do find a stable intermediate  
349 with metaphosphate ion in the gas-phase, however, it is  $\sim 21.2$  kcal/mol higher in energy  
350 than the reactant state—which is much higher than the free-energy difference. This can be  
351 explained on the basis that when metaphosphate breaks from the ATP molecule, *six* vibra-  
352 tional degrees of freedom are converted to *three* translational and *three* rotational degrees  
353 of freedom; hence, increasing its entropy. The gain in entropy stabilizes the metaphosphate  
354 intermediate in the gas-phase. We mention in passing that several previous theoretical  
355 studies have shown that gas-phase hydrolysis of phosphates proceeds through a dissociative  
356 mechanism involving a formation of metaphosphate ion as a stable intermediate.<sup>16,18,24</sup>

357 We also find that the Adenosine group plays a crucial role in the hydrolysis of ATP in  
358 the gas-phase, by providing a pseudo-solvation environment. Thus, stabilizing the reac-  
359 tion intermediate and facilitating hydrolysis of ATP by promoting intra-molecular hydrogen  
360 transfer. This is evident from the long-range proton-shuttling involving a nitrogen atom (in  
361 the five-membered ring) from the Adenine group, the nucleophilic water molecule and the  $\gamma$ -

362 and  $\beta$ - oxygens of the tri-phosphate group observed during the metadynamics run. Nitrogen  
363 in the five-membered ring of the Adenine group acts as the temporary resting place for the  
364 proton from the water molecule or the tri-phosphate group; thus helping in the dynamic  
365 rearrangement and transfer of proton. In order to capture the long-range motion of the  
366 protons, we plot the sum of coordination number of oxygen atoms involved in this process  
367 (denoted as O1,O2,O3 and O4 in Figure 8) with the hydrogens (denoted as H1, H2, H3 and  
368 H4 in Figure 8) that are involved in the process. We define the O-H coordination in the  
369 caption of Figure 8. Initially at  $T1=0fs$ , the hydrogens are placed on the native oxygens,  
370 i.e.; H1 is bonded with O1; H2 and H3 are bonded with O2 (or water oxygen, Ow); and  
371 H4 is bonded with O4. Hence, the coordination-number has its maximum value of  $\sim 3$ . At  
372  $T2\sim 3000fs$ , there is a drop in the O-H coordination number from  $\sim 1$  to  $\sim 0$ . This happens  
373 because there is transfer of H3 from O2 to the nitrogen atom of the Adenine ring, H4 from  
374 O4 to O2, and H1 from O1 to O3. Similarly, we show several intermediate structures during  
375 the gas-phase ATP hydrolysis in Figure 8 depicting various proton transfer events.

## 376 **B. Hydrolysis of H-ATP in the aqueous-phase**

377 We now elaborate on the findings of H-ATP hydrolysis in the aqueous phase. Although,  
378 we began this study with a fully protonated ATP molecule, after *ab initio* MD equilibration  
379 only two protons on the  $\gamma$  oxygens were left and rest of them were solvated in the aqueous  
380 solution (see snapshot ‘1’ in Figure 9). This suggests that H-ATP in these conditions tends  
381 to exist as divalent ions in the bulk solution. At higher pH conditions it may be present as  
382 a trivalent or a tetravalent ion.<sup>36,37,79</sup>

383 We plot the restricted free-energy surface for the aqueous-phase hydrolysis of H-ATP in  
384 Figure 2b obtained by performing metadynamics simulation along certain collective vari-  
385 ables. We define the *two* collective variables used in this study in Sec. II B 2. CV1 is related  
386 to the breaking and re-formation of bond between  $P_\gamma-O_{\beta b}$  and CV2 is related to the attack  
387 of nucleophilic water molecule. In the aqueous-phase simulations it could be any one of the  
388 water molecules surrounding the H-ATP molecule.

389 Unlike the gas-phase simulations, the free-energy surface obtained in the aqueous phase  
390 simulations is extremely rugged; which can be attributed to the presence of solvent co-  
391 ordinates in CV2. We find an overall barrier of  $\sim 37.7$  kcal/mol for the aqueous-phase

392 hydrolysis of H-ATP—which is  $\sim 5$  kcal/mol higher than the gas-phase simulations. This  
393 can be explained on the basis of well-known ‘cage-effect’,<sup>80,81</sup> which we elaborate below. The  
394 cage-effect also leads to a much higher free-energy barrier for the first-step in the aqueous-  
395 phase hydrolysis ( $\sim 33.5$  kcal/mol) compared to the gas-phase hydrolysis ( $\sim 20.6$  kcal/mol).

396 We find that the free-energy barrier for the second step of the aqueous-phase hydrolysis  
397 ( $\sim 5.3$  kcal/mol) is much smaller than the gas-phase hydrolysis ( $\sim 31.3$  kcal/mol). This is  
398 because, the attacking water molecule in the gas-phase hydrolysis has an extremely large  
399 entropic space to manoeuvre before it attaches itself to the metaphosphate. On the other  
400 hand, the leaving metaphosphate in the aqueous-phase hydrolysis is surrounded by the  
401 ‘cage’ of reactant water molecules which increases the probability of reacting and forming  
402 the orthophosphate product.

403 To better understand the mechanism of aqueous-phase H-ATP hydrolysis, we plot various  
404 parameters (such as collective variables, angles etc.) during the metadynamics trajectory.  
405 We also provide movie of the metadynamics trajectory in Supplementary Information (see  
406 Figure S6). Just like the gas-phase simulations, we observe dynamic rearrangement of the  
407 protons. However, in the aqueous-phase simulations it is the surrounding water molecules  
408 which play an active role instead of the Adenosine group. The proton diffuses in the solvent  
409 through Grotthuss mechanism.<sup>82</sup> At different instances of time, we observe the formation of  
410 Zundel cation<sup>83</sup> and Eigen cation.<sup>84</sup> The complex nature of the hydrated proton has been  
411 well documented before.<sup>85</sup>

412 We plot the evolution of collective variables *vs* metadynamics simulation time in Figure  
413 10. And, we also plot the sum of  $\angle$  O-P-O ( $\angle\theta$ ) of the terminal  $\text{PO}_3$  entity *vs* metadynamics  
414 time in Figure 11. Unlike the gas-phase simulations, both Figures 10 and 11 show large  
415 fluctuations in CV1 and  $\angle\theta$ , respectively. CV1 fluctuates between a value of  $\sim 0.9$  to  $\sim 0.2$   
416 several times in between 9 ps to 18.5 ps of the metadynamics time. At the same instances,  
417 the  $\angle\theta$  fluctuates between  $\sim 340^\circ$  to  $360^\circ$ . This suggests that  $\text{P}_\gamma\text{-O}_{\beta b}$  bond breaks and  
418 reforms—and terminal  $\text{PO}_3$  goes from a tetrahedral geometry to a planar geometry—several  
419 times during this period. We show these events in Figure 9 (snapshots ‘2’ and ‘3’). In the  
420 gas-phase study, once  $\text{P}_\gamma\text{-O}_{\beta b}$  bond breaks, we observe no recombination between the  
421 two dissociated species. This is because once the molecule has gained enough energy to  
422 leave, there is no motivation for it to go back. However, in the aqueous-phase hydrolysis,  
423 the dissociated species collides with the solvent molecules; and therefore have the tendency

424 to come back and recombine. This process of leaving and recombining occurs until the  
425 intermediate makes its way through the solvent. The phenomena is known as ‘cage-effect’.<sup>86</sup>  
426 Thus, the high free energy barrier for the first step in the case of aqueous-phase hydrolysis  
427 compared to the hydrolysis in the gas-phase can be attributed to the cage-effect.

428 At  $\sim 18.79$  ps,  $P_\gamma$  finally breaks its bond with  $O_{\beta b}$  as indicated by the decrease in CV1  
429 from  $\sim 0.8$  to  $\sim 0.1$  (see Figure 10 and snapshot ‘4’ in Figure 9). At the same instant, as  
430 shown in Figure 11,  $\angle\theta$  goes from  $\sim 340^\circ$  to  $360^\circ$ , i.e., a planar metaphosphate is formed.  
431 The lytic water loses its proton to the bridging oxygen,  $O_{\beta b}$ , and is involved in a network of  
432 hydrogen bond with two assisting water molecules (shown in yellow and green in snapshot  
433 ‘5’ of Figure 9) and one of the  $\gamma$  oxygens.

434 At  $\sim 21.74$  ps, the lytic water finally attaches itself to metaphosphate to form orthophos-  
435 phate, losing its proton to the nearby water molecule (shown in yellow in snapshot ‘6’ of  
436 Figure 9). At  $\sim 22.35$  ps, the orthophosphate ion gains protons from the solvent molecules to  
437 finally form orthophosphoric acid (see snapshot ‘7’ in Figure 9). The mechanism explained  
438 above is consistent with the solvent-assisted catalysis where nearby water molecules plays  
439 a role of general base helping in dynamic rearrangement of protons; in agreement with the  
440 previous studies.<sup>9,12</sup>

441 Figures 10 and 11 suggests that the metaphosphate intermediate is present for an ex-  
442 tremely short period of time. Therefore, it is difficult to discern between dissociative and  
443 concerted mechanism. However, Figures 10 and 11 also suggests that a metaphosphate in-  
444 termediate is formed first and then the lytic water attaches itself to metaphosphate, pointing  
445 towards a  $S_N1$ -type dissociative mechanism in the aqueous-phase. This is also supported by  
446 the MOFJ plot shown in Figure 5b.

### 447 C. Hydrolysis of Mg-ATP and Ca-ATP in the aqueous-phase

448 We now present our findings of Mg-ATP and Ca-ATP hydrolysis in the aqueous-phase.  
449 Both Mg and Ca ions are found to coordinate with ATP in our body.<sup>87</sup> In these simulations  
450 we replace two  $H^+$  ions—one on the  $\gamma$  oxygen and the other on  $\beta$  oxygen of the triphosphate  
451 tail—with the divalent ions. As before, we find that the triphosphate tail loses its protons  
452 to the bulk solvent during the equilibration runs to form a divalent ion. Interestingly, after  
453 the equilibration runs, Mg ion remains chelated to the  $\gamma$  and  $\beta$  oxygens (see snapshot ‘1’

454 in Figure 13); whereas Ca ion shifts to  $\beta$  and  $\alpha$  oxygens (see snapshot ‘1’ in Figure 15). A  
455 possible reason for this is that Mg and Ca ions prefer to have different coordination with the  
456 nucleophilic water oxygens in the aqueous-phase. The hydrated Mg ions is usually found to  
457 be six-coordinate with an average Mg-O distance of 2.09 Å, in an octahedron configuration,  
458 in the aqueous solution; whereas Ca ion is found to be eight-coordinate with an average  
459 Ca-O distance of 2.42 Å, in a square antiprism configuration.<sup>88-91</sup> Because of the larger size  
460 of Ca ion it prefers to fit into the pocket of  $\beta$  and  $\alpha$  oxygens.

461 Similar to the previous study,<sup>12</sup> we find that Mg(II) ion remains chelated to the  $\gamma$  and  
462  $\beta$  oxygens throughout the hydrolysis process. Whereas, Ca(II) ion changed its chelation  
463 from bidentate to mono-dentate during the process. Also, we find both Mg and Ca ions  
464 maintained its coordination with the oxygens throughout the process. Mg ion showed an  
465 average coordination of *six*, whereas Ca ion showed an average coordination of *seven* with the  
466 nearby oxygens. This is evident from the sharp radial distribution peaks and coordination  
467 number plots in Supplementary Information (see Figures S8, S9 and S10). We find an  
468 average Mg-O distance of 2.1 Å and an average Ca-O distance of 2.41 Å, agreeing well with  
469 the experimental values of average coordination distances in the aqueous-phase.<sup>88-91</sup>

470 We present the restricted free-energy surface for the aqueous-phase hydrolysis of Mg-  
471 ATP and Ca-ATP in Figures 2c and 2d, respectively. The collective variables along which  
472 the repulsive potentials are added are defined in Sec. II B 2. We find an overall barrier  
473 of  $\sim 30.6$  kcal/mol and  $\sim 30.3$  kcal/mol, respectively, for the hydrolysis of Mg-ATP and  
474 Ca-ATP. Because the difference in barriers is within the natural error of 1 kcal/mol in  
475 our metadynamics simulations, we are not able to decide which one has a lower barrier.  
476 Additionally, we do not compare these barriers to experimental results because of several  
477 reasons. First, it is difficult to emulate exact experimental conditions in simulations. Second,  
478 PBE functional used in this work is accurate to within 0.2 eV. Third, the quantum effects  
479 associated with proton transfer are not accounted for in this work. Therefore, we focus on  
480 qualitative findings and comparisons rather than quantitative aspects of the simulation. We,  
481 however, mention in passing that previous experimental studies report a barrier between 26-  
482 31 kcal/mol<sup>38,92,93</sup> and previous in-silico studies report a barrier between 29-35 kcal/mol<sup>9-13,16</sup>  
483 for the non-enzymatic hydrolysis of tri-phosphates in the aqueous-phase.

484 Unlike the gas-phase and the aqueous-phase H-ATP simulations, we find that the reaction  
485 proceeds in a single-step and no intermediate is observed in the aqueous-phase hydrolysis

486 of Mg-ATP and Ca-ATP. However, we find that several features of the free-energy surface  
487 are similar to the aqueous-phase H-ATP simulations. First, the free-energy surface is quite  
488 rugged in comparison to the gas-phase hydrolysis which can be attributed to the solvent  
489 coordinates. Second, the barrier for the first-step (or the only step) is much higher than the  
490 gas-phase hydrolysis process. This is due to the presence of cage of reactant water molecules  
491 which collides with the dissociated metaphosphate causing it to go back and recombine.  
492 After several attempts, the metaphosphate is finally able to gain enough energy to make its  
493 way through the cage.

494 We now elaborate on the mechanistic aspects of hydrolysis by plotting evolution of col-  
495 lective variables in Figures 12 and 14 for Mg and Ca ions, respectively. We also provide  
496 snapshots at different instances of metadynamics time in Figures 13 and 15 along with movies  
497 of the metadynamics trajectory in Supplementary Information (see Figures S11 and S12).  
498 Similar to the aqueous-phase hydrolysis of H-ATP, we find nearby water molecules assisting  
499 in the hydrolysis process by facilitating dynamic rearrangement of protons. For example,  
500 we refer the reader to Figure 13 where we show snapshots of metadynamics trajectory for  
501 the hydrolysis of Mg-ATP. At  $\sim 17.05$  ps, the lytic water (shown in purple) attaches itself to  
502 metaphosphate ion forming an orthophosphate moiety (snapshot ‘3’), and gets involved in  
503 a network of hydrogen bond with five other water molecules (shown in yellow, blue, orange,  
504 brown, and pink in snapshot ‘4’). The proton diffuses through Grotthuss mechanism along  
505 a chain of *five* water molecules to the oxygen of the  $\text{HPO}_4^{2-}$  ion (snapshot ‘5’).

506 CV1 is directly related to the terminal phospho-anhydride bond ( $P_\gamma - O_{\beta b}$ ), and large  
507 fluctuations of CV1 suggests breaking and reformation of the  $P_\gamma - O_{\beta b}$  bond, which is the  
508 characteristic of well-known “cage effect”. Similar to H-ATP hydrolysis in the aqueous  
509 solution, our results show cage-effect in the hydrolysis of Mg-ATP and Ca-ATP, evident  
510 from the large fluctuations of CV1 as shown in Figures 12 and 14; respectively.

511 Similar to the aqueous-phase hydrolysis of H-ATP, it is difficult to discern between dis-  
512 sociative and concerted mechanism in case of Mg-ATP and Ca-ATP. However, as argued  
513 before, Figure 12 suggests breaking of terminal phospho-anhydride bond first and then at-  
514 tack of nucleophilic water, pointing towards a possible  $\text{S}_{\text{N}}1$ -type dissociative mechanism in  
515 the aqueous-phase hydrolysis of Mg-ATP. In contrast, in the case of aqueous-phase hydroly-  
516 sis of Ca-ATP, Figure 14 shows both breaking of terminal phospho-anhydride bond and  
517 attack of lytic water happens simultaneously, indicating to a possible concerted mechanism.

518 At  $\sim 14.10$  ps, the distance between  $P_\gamma$  and  $O_{\beta b}$  is nearly equal to the distance between the  
519  $P_\gamma$  and  $O_w$  of the lytic water. At the same instant the geometry of the leaving metaphos-  
520 phate is planar (see Figure S14 in Supplementary Information), which is the signature of  
521 Walden’s inversion or  $S_N2$ -type concerted mechanism. These conclusions are well supported  
522 by the MOFJ plots in Figures 5c and 5d. For hydrolysis of Mg-ATP, the reactive trajec-  
523 tory is towards the dissociative corner in MOFJ plot. Whereas, the reactive event proceeds  
524 through the diagonal of the MOFJ plot in the case of hydrolysis of Ca-ATP.

525 The overall barriers for the aqueous-phase hydrolysis of divalent ions are much lower  
526 than the aqueous-phase ( $\sim 38$  kcal/mol) hydrolysis of H-ATP suggesting a clear catalytic  
527 effect of the divalent ions. A possible reason for this is the increased electrophilicity of  
528 the terminal  $PO_3$  after breaking of the terminal phospho-anhydride bond. This is evident  
529 from the Figures S15 and S16 in supplementary information which shows that the charge on  
530 the terminal  $PO_3$  moiety becomes less negative every time  $P_\gamma - O_{\beta b}$  bond breaks; making  
531 it easy for the nucleophilic water molecule to attack. This was not observed in the case  
532 of aqueous-phase hydrolysis of H-ATP (see Figure S7 in supplementary information). The  
533 discussion above suggests that divalent ions facilitate the attack of the nucleophilic water  
534 molecule which is in agreement to the previous studies.<sup>94-97</sup>

#### 535 IV. SUMMARY AND CONCLUSIONS

536 In this work, we study hydrolysis of ATP in the gas-phase and the aqueous-phase by  
537 performing *ab initio* MD simulations with an enhanced sampling technique. In gas-phase  
538 we studied hydrolysis of fully protonated ATP molecule. In the aqueous-phase, we studied  
539 hydrolysis of ATP coordinated with: a) *two*  $H^+$  ions (H-ATP), b)  $Mg^{2+}$  (Mg-ATP) and c)  
540  $Ca^{2+}$  (Ca-ATP).

541 We found that hydrolysis in the gas-phase proceeds *via* dissociative mechanism through  
542 a stable metaphosphate ion. Interestingly, we found that the Adenosine group of the ATP  
543 molecule plays a crucial role during the hydrolysis reaction. The Adenine group played  
544 the role of a general base by accepting a proton from the water molecule, which in turn  
545 accepts the proton from the leaving metaphosphate group; thus helping in the dissociation  
546 of the ATP molecule. The final proton transfer to the phosphate oxygen occurs similarly  
547 involving the nitrogen on the Adenine ring, orthophosphate moiety and the  $\beta$ -phosphate

548 oxygen. These results suggest that small molecules like monophosphate esters, pyrophos-  
549 phates and truncated versions like MTP (methyl triphosphate) may not serve as good models  
550 for studying hydrolysis of ATP, GTP and, similar nucleotides; especially in an enzymatic  
551 pocket where the environment for hydrolysis is hydrophobic and is similar to the gas-phase  
552 environment.

553 On comparison of our gas-phase study with that of aqueous-phase hydrolysis of H-ATP,  
554 we observed several differences. First, the presence of cage of solvent molecules increases  
555 the stability of the terminal phospho-anhydride bond. The leaving metaphosphate moiety  
556 recombined with the bridging oxygen many times before finally getting captured by a nucle-  
557 ophilic water molecule. This was also the reason for higher free-energy barrier for the first  
558 step for ATP hydrolysis in the aqueous solution compared to that in the gas-phase. Second,  
559 although we found that hydrolysis of both H-ATP in the gas-phase and the aqueous solution  
560 proceeded *via* S<sub>N</sub>1-type dissociative mechanism involving formation of a metaphosphate in-  
561 termediate; however, in the case of aqueous-phase the lifetime of the intermediate was much  
562 shorter than that in the gas-phase. Third, in the aqueous-phase, we found that the solvent  
563 plays an active role in assisting the hydrolysis process by proton transfer through Grotthuss  
564 mechanism. In contrast, in the gas-phase, we found that the Adenine group of the ATP  
565 molecule play an active role as a base helping in the hydrolysis process.

566 We obtained much lower free-energy barriers for the aqueous-phase hydrolysis of ATP  
567 coordinated with divalent ions (Mg<sup>2+</sup> and Ca<sup>2+</sup>) compared to that in the aqueous-phase  
568 hydrolysis of ATP coordinated with only H<sup>+</sup> ions—which suggests a clear catalytic effect of  
569 the divalent ions. This can be attributed to the increased electrophilicity of the leaving PO<sub>3</sub>  
570 moiety in the case of divalent ions, which facilitates attack of the nucleophilic water molecule.  
571 Interestingly, we find a single-step dissociative-type mechanism for Mg-ATP, whereas, the  
572 hydrolysis in case of Ca-ATP proceeded through a S<sub>N</sub>-2-type concerted pathway.

## 573 ACKNOWLEDGMENTS

574 We acknowledge support from the High Performance Computing center at IITK. VA ac-  
575 knowledges the funding support from IITK (initiation grant). RS acknowledges the financial  
576 support from the Ministry of Human Resource Development, Govt of India. We also thank  
577 Prof. Nisanth N. Nair and Prof. Sanjeev Garg for stimulating discussions on this topic.

578 **SUPPORTING INFORMATION**

579 Additional supporting information may be found online in the Supporting Information  
580 section at the end of this article.

- 
- 581 [1] J. R. Knowles, Enzyme-Catalyzed Phosphoryl Transfer Reactions, Annual Review of Biochem-  
582 istry **49**, 877 (1980).
- 583 [2] J. K. Lassila, J. G. Zalatan, and D. Herschlag, Biological phosphoryl-transfer reactions: un-  
584 derstanding mechanism and catalysis, Annual review of biochemistry **80**, 669 (2011).
- 585 [3] P. D. Boyer, the Atp Synthase-a Splendid Molecular Machine, Annual Review of Biochemistry  
586 **66**, 717 (1997).
- 587 [4] F. Westheimer, Why nature chose phosphates, Science **235**, 1173 (1987).
- 588 [5] A. L. Buchachenko, D. A. Kuznetsov, and N. N. Breslavskaya, Chemistry of enzymatic ATP  
589 synthesis: An insight through the isotope window, Chemical Reviews **112**, 2042 (2012).
- 590 [6] J. E. Walker, The ATP synthase: The understood, the uncertain and the unknown, Biochem-  
591 ical Society Transactions **41**, 1 (2013).
- 592 [7] S. C. Kamerlin, P. K. Sharma, R. B. Prasad, and A. Warshel, Why nature really chose  
593 phosphate, Quarterly reviews of biophysics **46**, 1 (2013).
- 594 [8] S. J. Admiraal and D. Herschlag, Mapping the transition state for atp hydrolysis: implications  
595 for enzymatic catalysis, Chemistry & biology **2**, 729 (1995).
- 596 [9] B. L. Grigorenko, , A. V. Rogov, and A. V. Nemukhin, Mechanism of triphosphate hydrolysis  
597 in aqueous solution: Qm/mm simulations in water clusters, Journal of Physical Chemistry B  
598 **110**, 4407 (2006).
- 599 [10] J. Akola and R. Jones, Atp hydrolysis in water- a density functional study, The Journal of  
600 Physical Chemistry B **107**, 11774 (2003).
- 601 [11] C. B. Harrison and K. Schulten, Quantum and classical dynamics simulations of atp hydrolysis  
602 in solution, Journal of chemical theory and computation **8**, 2328 (2012).
- 603 [12] R. Glaves, G. Mathias, and D. Marx, Mechanistic insights into the hydrolysis of a nucleoside  
604 triphosphate model in neutral and acidic solution, Journal of the American Chemical Society  
605 **134**, 6995 (2012).
- 606 [13] C. Wang, W. Huang, and J.-L. Liao, Qm/mm investigation of atp hydrolysis in aqueous  
607 solution, The Journal of Physical Chemistry B **119**, 3720 (2015).
- 608 [14] J. Florián and A. Warshel, Phosphate ester hydrolysis in aqueous solution: associative versus  
609 dissociative mechanisms, The Journal of Physical Chemistry B **102**, 719 (1998).

- 610 [15] J. Åqvist, K. Kolmodin, J. Florian, and A. Warshel, Mechanistic alternatives in phosphate  
611 monoester hydrolysis: what conclusions can be drawn from available experimental data?,  
612 *Chemistry & biology* **6**, R71 (1999).
- 613 [16] Y. N. Wang, I. A. Topol, J. R. Collins, and S. K. Burt, Theoretical Studies on the Hydrolysis  
614 of Mono-Phosphate and Tri-Phosphate in Gas Phase and Aqueous Solution, *Journal of the*  
615 *American Chemical Society* **125**, 13265 (2003).
- 616 [17] M. E. Colvin, E. Evleth, and Y. Akacem, Quantum Chemical Studies of Pyrophosphate Hy-  
617 drolysis, *Journal of the American Chemical Society* **117**, 4357 (1995).
- 618 [18] C. H. Hu and T. Brinck, Theoretical Studies of the Hydrolysis of the Methyl Phosphate Anion,  
619 *Journal of Physical Chemistry A* **103**, 5379 (1999).
- 620 [19] J. R. Johnson and I. Panas, Water adsorption and hydrolysis in the Si<sub>2</sub>O<sub>4</sub>, P<sub>2</sub>O<sub>5</sub> and P<sub>4</sub>O<sub>10</sub>  
621 systems - Essential roles of the phosphate system in biosynthesis, *Chemical Physics* **276**, 45  
622 (2002).
- 623 [20] W. J. McCarthy, D. M. Smith, L. Adamowicz, H. Saint-Martin, and I. Ortega-Blake, An ab  
624 initio study of the isomerization of Mg- and Ca-pyrophosphates, *Journal of the American*  
625 *Chemical Society* **120**, 6113 (1998).
- 626 [21] E. Franzini, P. Fantucci, and L. De Gioia, Density Functional Theory investigation of guanosine  
627 triphosphate models: Catalytic role of Mg<sup>2+</sup> ions in phosphate ester hydrolysis, *Journal of*  
628 *Molecular Catalysis A: Chemical* **204-205**, 409 (2003).
- 629 [22] W. Li, T. Rudack, K. Gerwert, F. Gräter, and J. Schlitter, Exploring the multidimensional  
630 free energy surface of phosphoester hydrolysis with constrained qm/mm dynamics, *Journal of*  
631 *chemical theory and computation* **8**, 3596 (2012).
- 632 [23] J. Florián and A. Warshel, A fundamental assumption about oh-attack in phosphate ester  
633 hydrolysis is not fully justified, *Journal of the American Chemical Society* **119**, 5473 (1997).
- 634 [24] B. Ma, C. Meredith, and H. F. Schaefer III, The quest for a metaphosphate intermediate.  
635 the mechanisms for hydrolysis of pyrophosphates with and without catalysis, *The Journal of*  
636 *Physical Chemistry* **99**, 3815 (1995).
- 637 [25] H. Saint-Martin, L. E. Ruiz-Vicent, A. Ramírez-Solís, and I. Ortega-Blake, Toward an un-  
638 derstanding of the hydrolysis of mg- ppi. an ab initio study of the isomerization reactions of  
639 neutral and anionic mg- pyrophosphate complexes, *Journal of the American Chemical Society*  
640 **118**, 12167 (1996).

- 641 [26] R. J. Dawson and K. P. Locher, Structure of a bacterial multidrug abc transporter, *Nature*  
642 **443**, 180 (2006).
- 643 [27] M. L. Oldham and J. Chen, Snapshots of the maltose transporter during atp hydrolysis,  
644 *Proceedings of the National Academy of Sciences* **108**, 15152 (2011).
- 645 [28] E. Kobayashi, K. Yura, and Y. Nagai, Distinct conformation of atp molecule in solution and  
646 on protein, *Biophysics* **9**, 1 (2013).
- 647 [29] M. Prieß, H. Göddeke, G. Groenhof, and L. V. Schafer, Molecular mechanism of atp hydrolysis  
648 in an abc transporter, *ACS central science* **4**, 1334 (2018).
- 649 [30] A. F. Voter, F. Montalenti, and T. C. Germann, Extending the time scale in atomic simulaiton  
650 of materials, *Annual Review of Materials Research* **32**, 321 (2002).
- 651 [31] A. Voter, Hyperdynamics: Accelerated molecular dynamics of infrequent events, *Physical*  
652 *Review Letters* **78**, 3908 (1997).
- 653 [32] A. F. Voter, A method for accelerating the molecular dynamics simulation of infrequent events,  
654 *Journal of Chemical Physics* **106**, 4665 (1997).
- 655 [33] A. Voter, Parallel replica method for dynamics of infrequent events, *Physical Review B* **57**,  
656 R13985 (1998).
- 657 [34] M. R. Sørensen and A. F. Voter, Temperature-accelerated dynamics for simulation of infre-  
658 quent events, *The Journal of Chemical Physics* **112**, 9599 (2000).
- 659 [35] A. Laio and M. Parrinello, Escaping free-energy minima, *Proceedings of the National Academy*  
660 *of Sciences* **99**, 12562 (2002).
- 661 [36] R. Tribolet and H. Sigel, Influence of the protonation degree on the self-association properties  
662 of adenosine 5'-triphosphate (ATP), *European Journal of Biochemistry* **170**, 617 (1988).
- 663 [37] P. Wang, J. L. Oscarson, R. M. Izatt, G. D. Watt, and C. D. Larsen, Thermodynamic pa-  
664 rameters for the interaction of adenosine 5'-diphosphate, and adenosine 5'-triphosphate with  
665  $Mg^{2+}$  from 323.15 to 398.15 K, *Journal of Solution Chemistry* **24**, 989 (1995).
- 666 [38] M. Taqui Khan and M. Srinivas Mohan, Kinetics of adenosine-5'-triphosphate hydrolysis,  
667 *Journal of Inorganic and Nuclear Chemistry* **36**, 707 (1974).
- 668 [39] S. Meyerson, E. S. Kuhn, F. Ramirez, and J. F. Marecek, Hydrolysis of Adenosine 5'-  
669 Triphosphate: An Isotope-Labeling Study, *Journal of the American Chemical Society* **104**,  
670 7231 (1982).

- 671 [40] J. Wang, R. M. Wolf, J. W. Caldwell, P. A. Kollman, and D. A. Case, Development and  
672 testing of a general amber force field, *Journal of computational chemistry* **25**, 1157 (2004).
- 673 [41] A.-R. Allouche, Gabedit-A graphical user interface for computational chemistry softwares,  
674 *Journal of Computational Chemistry* **32**, 174 (2011).
- 675 [42] M. Korth, M. Pitoňák, J. Řezáč, and P. Hobza, A transferable H-bonding correction for  
676 semiempirical quantum-chemical methods, *Journal of Chemical Theory and Computation* **6**,  
677 344 (2010).
- 678 [43] J. J. P. Stewart, Mopac: A semiempirical molecular orbital program, *Journal of Computer-*  
679 *Aided Molecular Design* **4**, 1 (1990).
- 680 [44] A. D. Becke, Density-functional exchange-energy approximation with correct asymptotic be-  
681 havior, *Physical Review A* **38**, 3098 (1988).
- 682 [45] C. T. Lee, W. T. Yang, and R. G. Par, Development of the {Colle-Salvetti} Correlation-Energy  
683 Formula into a Functional of the Electron-Density, *Physical Review B* **37**, 785 (1988).
- 684 [46] B. Miehlich, A. Savin, H. Stoll, and H. Preuss, Results obtained with the correlation energy  
685 density functionals of becke and Lee, Yang and Parr, *Chemical Physics Letters* **157**, 200  
686 (1989).
- 687 [47] G. A. Petersson and M. A. Al-Laham, A complete basis set model chemistry. II. Open-shell  
688 systems and the total energies of the first-row atoms, *The Journal of Chemical Physics* **94**,  
689 6081 (1991).
- 690 [48] G. A. Petersson, A. Bennett, T. G. Tensfeldt, M. A. Al-Laham, W. A. Shirley, and  
691 J. Mantzaris, A complete basis set model chemistry. I. The total energies of closed-shell atoms  
692 and hydrides of the first-row elements, *The Journal of Chemical Physics* **89**, 2193 (1988).
- 693 [49] T. Miyazaki, Y. Kameda, Y. Umabayashi, H. Doi, Y. Amo, and T. Usuki, Conformation of  
694 ATP and ADP molecules in aqueous solutions determined by high-energy X-ray diffraction,  
695 *Journal of Solution Chemistry* **43**, 1487 (2014).
- 696 [50] E. Lindahl, B. Hess, and D. Van Der Spoel, Gromacs 3.0: a package for molecular simulation  
697 and trajectory analysis, *Molecular modeling annual* **7**, 306 (2001).
- 698 [51] H. J. C. Berendsen, D. van der Spoel, and R. van Drunen, GROMACS: a message-passing par-  
699 allel molecular dynamics implementation, *Computer physics communications* **91**, 43 (1995).
- 700 [52] H. Berendsen, J. Grigera, and T. Straatsma, The missing term in effective pair potentials,  
701 *Journal of Physical Chemistry* **91**, 6269 (1987).

- 702 [53] A. W. S. da Silva and W. F. Vranken, Acypype - antechamber python parser interface, BMC  
703 Research Notes **5**, 367 (2012).
- 704 [54] D. J. Evans and B. L. Holian, The nose–hoover thermostat, The Journal of chemical physics  
705 **83**, 4069 (1985).
- 706 [55] J. Hutter, M. Iannuzzi, F. Schiffmann, and J. Vandevondele, Cp2k: Atomistic simulations of  
707 condensed matter systems, Wiley Interdisciplinary Reviews: Computational Molecular Science  
708 10.1002/wcms.1159 (2014).
- 709 [56] M. J. Frisch, G. W. Trucks, H. B. Schlegel, G. E. Scuseria, M. A. Robb, J. R. Cheeseman,  
710 G. Scalmani, V. Barone, B. Mennucci, G. A. Petersson, H. Nakatsuji, M. Caricato, X. Li,  
711 H. P. Hratchian, A. F. Izmaylov, J. Bloino, G. Zheng, J. L. Sonnenberg, M. Hada, M. Ehara,  
712 K. Toyota, R. Fukuda, J. Hasegawa, M. Ishida, T. Nakajima, Y. Honda, O. Kitao, H. Nakai,  
713 T. Vreven, J. A. Montgomery Jr., J. E. Peralta, F. Ogliaro, M. Bearpark, J. J. Heyd, E. Broth-  
714 ers, K. N. Kudin, V. N. Staroverov, R. Kobayashi, J. Normand, K. Raghavachari, A. Rendell,  
715 J. C. Burant, S. S. Iyengar, J. Tomasi, M. Cossi, N. Rega, J. M. Millam, M. Klene, J. E. Knox,  
716 J. B. Cross, V. Bakken, C. Adamo, J. Jaramillo, R. Gomperts, R. E. Stratmann, O. Yazyev,  
717 A. J. Austin, R. Cammi, C. Pomelli, J. W. Ochterski, R. L. Martin, K. Morokuma, V. G.  
718 Zakrzewski, G. A. Voth, P. Salvador, J. J. Dannenberg, S. Dapprich, A. D. Daniels, O. Farkas,  
719 J. B. Foresman, J. V. Ortiz, J. Cioslowski, and D. J. Fox,.
- 720 [57] P. Hohenberg and W. Kohn, Inhomogeneous electron gas, Physical review **136**, B864 (1964).
- 721 [58] W. Kohn and L. J. Sham, Self-consistent equations including exchange and correlation effects,  
722 Physical review **140**, A1133 (1965).
- 723 [59] J. Kohanoff and N. Gidopoulos, Density functional theory: basics, new trends and applica-  
724 tions, Handbook of molecular physics and quantum chemistry **2**, 532 (2003).
- 725 [60] R. G. Parr, Density functional theory of atoms and molecules, in *Horizons of Quantum Chem-*  
726 *istry* (Springer, 1980) pp. 5–15.
- 727 [61] J. P. Perdew, K. Burke, and M. Ernzerhof, Generalized gradient approximation made simple,  
728 Physical Review Letters 10.1103/PhysRevLett.77.3865 (1996).
- 729 [62] B. G. LIPPERT, J. H. PARRINELLO, and MICHELE, A hybrid gaussian and plane wave  
730 density functional scheme, Molecular Physics **92**, 477 (1997).
- 731 [63] J. Vandevondele, M. Krack, F. Mohamed, M. Parrinello, T. Chassaing, and J. Hutter, Quick-  
732 step: Fast and accurate density functional calculations using a mixed Gaussian and plane

- waves approach, *Computer Physics Communications* **167**, 103 (2005).
- [64] S. Goedecker, M. Teter, and J. Hutter, Separable dual-space gaussian pseudopotentials, *Physical Review B* **54**, 1703 (1996).
- [65] C. Hartwigsen, S. Goedecker, and J. Hutter, Relativistic separable dual-space gaussian pseudopotentials from h to rn, *Physical Review B* **58**, 3641 (1998).
- [66] J. VandeVondele and J. Hutter, Gaussian basis sets for accurate calculations on molecular systems in gas and condensed phases, *Journal of Chemical Physics* **127**, 10.1063/1.2770708 (2007).
- [67] S. Grimme, J. Antony, S. Ehrlich, and H. Krieg, A consistent and accurate ab initio parametrization of density functional dispersion correction (dft-d) for the 94 elements h-pu, *The Journal of chemical physics* **132**, 154104 (2010).
- [68] M. Iannuzzi, A. Laio, and M. Parrinello, Efficient exploration of reactive potential energy surfaces using car-parrinello molecular dynamics, *Physical Review Letters* **90**, 238302 (2003).
- [69] A. Laio and F. L. Gervasio, Metadynamics: a method to simulate rare events and reconstruct the free energy in biophysics, chemistry and material science, *Reports on Progress in Physics* **71**, 126601 (2008).
- [70] A. Barducci, M. Bonomi, and M. Parrinello, *Metadynamics*, *Wiley Interdisciplinary Reviews: Computational Molecular Science* **1**, 826 (2011).
- [71] B. Ensing, A. Laio, M. Parrinello, and M. L. Klein, A recipe for the computation of the free energy barrier and the lowest free energy path of concerted reactions, *The journal of physical chemistry B* **109**, 6676 (2005).
- [72] V. Agarwal, P. J. Dauenhauer, G. W. Huber, and S. M. Auerbach, Ab initio dynamics of cellulose pyrolysis: Nascent decomposition pathways at 327 and 600 °C, *Journal of the American Chemical Society* **134**, 14958 (2012).
- [73] R. Sun, O. Sode, J. F. Dama, and G. A. Voth, Simulating Protein Mediated Hydrolysis of ATP and Other Nucleoside Triphosphates by Combining QM/MM Molecular Dynamics with Advances in Metadynamics, *Journal of Chemical Theory and Computation* **13**, 2332 (2017).
- [74] M. McCullagh, M. G. Saunders, and G. A. Voth, Unraveling the mystery of ATP hydrolysis in actin filaments, *Journal of the American Chemical Society* **136**, 13053 (2014).
- [75] N. Vithani, S. Batra, B. Prakash, and N. N. Nair, Elucidating the GTP Hydrolysis Mechanism in FeoB: A Hydrophobic Amino-Acid Substituted GTPase, *ACS Catalysis* **7**, 902 (2017).

- 764 [76] A. Barducci, G. Bussi, and M. Parrinello, Well-tempered metadynamics: a smoothly converg-  
765 ing and tunable free-energy method, *Physical review letters* **100**, 020603 (2008).
- 766 [77] R. M. O’Ferrall, Relationships between e<sup>2</sup> and e<sup>1c</sup> b mechanisms of  $\beta$ -elimination, *Journal*  
767 *of the Chemical Society B: Physical Organic* , 274 (1970).
- 768 [78] W. P. Jencks, General acid-base catalysis of complex reactions in water, *Chemical reviews* **72**,  
769 705 (1972).
- 770 [79] F. Ramirez, J. F. Marecek, and J. Szamosi, Magnesium and Calcium Ion Effects on Hydrolysis  
771 Rates of Adenosine 5'-Triphosphate, *Journal of Organic Chemistry* **45**, 4748 (1980).
- 772 [80] J. Franck and E. Rabinowitsch, Some remarks about free radicals and the photochemistry of  
773 solutions, *Transactions of the Faraday Society* **30**, 120 (1934).
- 774 [81] E. Rabinowitch and W. Wood, The collision mechanism and the primary photochemical process  
775 in solutions, *Transactions of the Faraday Society* **32**, 1381 (1936).
- 776 [82] N. Agmon, The Grotthuss mechanism, *Chemical Physics Letters* **244**, 456 (1995).
- 777 [83] G. Zundel and H. Metzger, Energiebänder der tunnelnden überschuß-protonen in flüssigen  
778 säuren. eine ir-spektroskopische untersuchung der natur der gruppierungen h<sub>5</sub>o<sub>2</sub><sup>+</sup>, *Zeitschrift*  
779 *für Physikalische Chemie* **58**, 225 (1968).
- 780 [84] M. Eigen, Proton Transfer, Acid-Base Catalysis, and Enzymatic Hydrolysis, *Angewandte*  
781 *Chemie international edition* **3**, 1 (1964).
- 782 [85] D. Marx, M. E. Tuckerman, J. Hutter, and M. Parrinello, The nature of the hydrated excess  
783 proton in water, *Nature* **397**, 601 (1999).
- 784 [86] R. M. Noyes, A treatment of chemical kinetics with special applicability to diffusion controlled  
785 reactions, *The Journal of Chemical Physics* **1349**, 1349 (1954).
- 786 [87] A. P. Carvalho and B. Leo, Effects of ATP on the interaction of Ca<sup>++</sup>, Mg<sup>++</sup>, and K<sup>+</sup>  
787 with fragmented sarcoplasmic reticulum isolated from rabbit skeletal muscle., *The Journal of*  
788 *general physiology* **50**, 1327 (1967).
- 789 [88] C. W. Bock, A. Kaufman, and J. P. Glusker, Coordination of Water to Magnesium Cations,  
790 *Inorganic Chemistry* **33**, 419 (1994).
- 791 [89] F. C. Lightstone, E. Schwegler, R. Q. Hood, F. Gygi, and G. Galli, A first principles molec-  
792 ular dynamics simulation of the hydrated magnesium ion, *Chemical Physics Letters* **343**, 549  
793 (2001).

- 794 [90] I. Persson, Hydrated metal ions in aqueous solution: How regular are their structures?, Pure  
795 and Applied Chemistry **82**, 1901 (2010).
- 796 [91] A. K. Katz, J. P. Glusker, S. A. Beebe, and C. W. Bock, Calcium ion coordination: A  
797 comparison with that of beryllium, magnesium, and zinc, Journal of the American Chemical  
798 Society **118**, 5752 (1996).
- 799 [92] S. L. Friess, Rates and Energetics of Activation of the Acid-catalyzed Hydrolysis of Adenosine  
800 Triphosphate, Journal of the American Chemical Society **75**, 323 (1953).
- 801 [93] C. Kötting and K. Gerwert, Time-resolved FTIR studies provide activation free energy, ac-  
802 tivation enthalpy and activation entropy for GTPase reactions, Chemical Physics **307**, 227  
803 (2004).
- 804 [94] T. Rudack, F. Xia, J. Schlitter, C. Kötting, and K. Gerwert, The role of magnesium for  
805 geometry and charge in gtp hydrolysis, revealed by quantum mechanics/molecular mechanics  
806 simulations, Biophysical journal **103**, 293 (2012).
- 807 [95] M. A. van Bochove, G. Roos, C. F. Guerra, T. A. Hamlin, and F. M. Bickelhaupt, How mg<sup>2+</sup>  
808 ions lower the sn<sup>2</sup>@p barrier in enzymatic triphosphate hydrolysis, Chemical Communications  
809 **54**, 3448 (2018).
- 810 [96] A. S. Mildvan and C. M. Grisham, The role of divalent cations in the mechanism of enzyme  
811 catalyzed phosphoryl and nucleotidyl transfer reactions, in *Biochemistry* (Springer, 1974) pp.  
812 1–21.
- 813 [97] A. Kirby and W. Jencks, The reactivity of nucleophilic reagents toward the p-nitrophenyl  
814 phosphate dianion<sup>1</sup>, Journal of the American Chemical Society **87**, 3209 (1965).

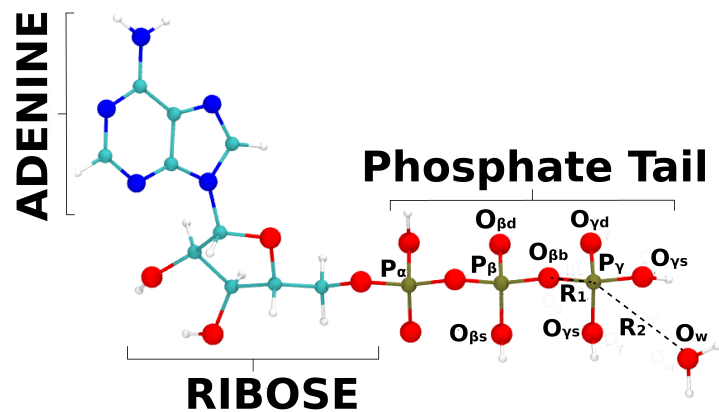


FIG. 1. Representative figure of adenosine triphosphate (H-ATP) molecule along with a water molecule. The water oxygen is denoted as  $O_w$ .  $R_1$  is the distance between  $P_\gamma$  and  $O_{\beta b}$ ; and  $R_2$  is the distance between  $O_w$  and  $P_\gamma$ . Hydrogen atoms are shown in white, oxygen atoms in red, phosphorus atoms in tan, carbon atoms in cyan and nitrogen atoms in blue.

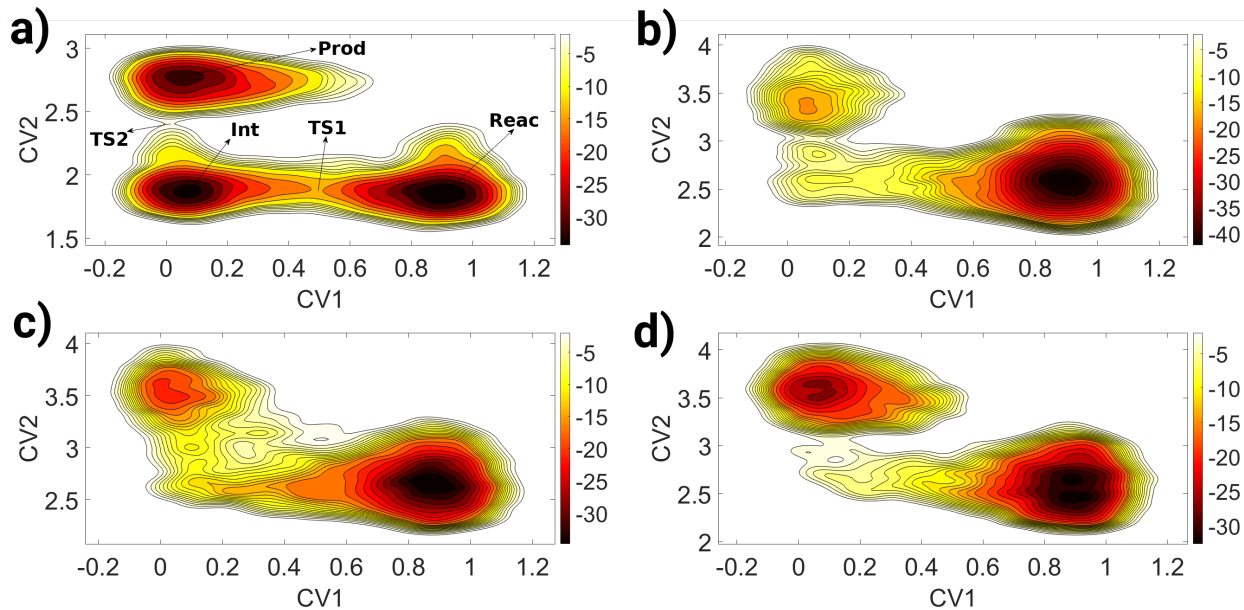


FIG. 2. Restricted free energy surface constructed from repulsive potentials added during a metadynamics run for studying hydrolysis of **a)** H-ATP in the gas-phase, **b)** H-ATP in the aqueous-phase, **c)** Mg-ATP in the aqueous-phase, and **d)** Ca-ATP in the aqueous-phase. See Sec. II B 2 for definitions of CV1 and CV2. The figure only justifies the forward reaction barriers as the simulations were stopped before the final product basin could fully fill. The color coding for the contours are shown on the right side of the panel with units of energy in kcal/mol.

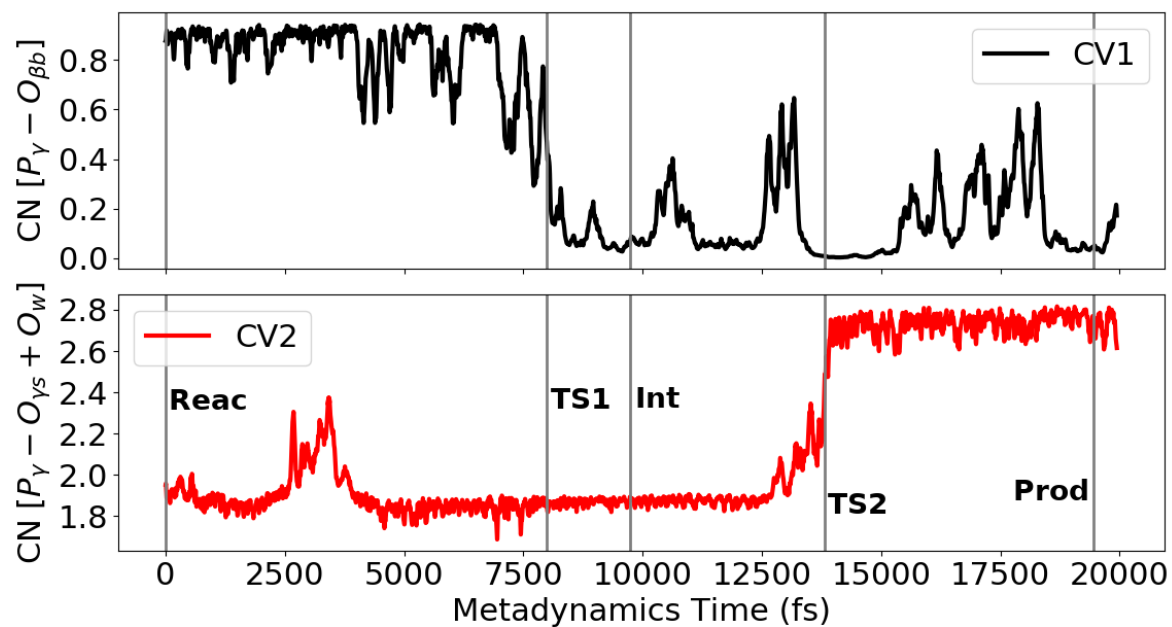


FIG. 3. Changes in collective variables during a metadynamics run for gas-phase hydrolysis of H-ATP. See Sec. II B 2 for definitions of CV1 and CV2.

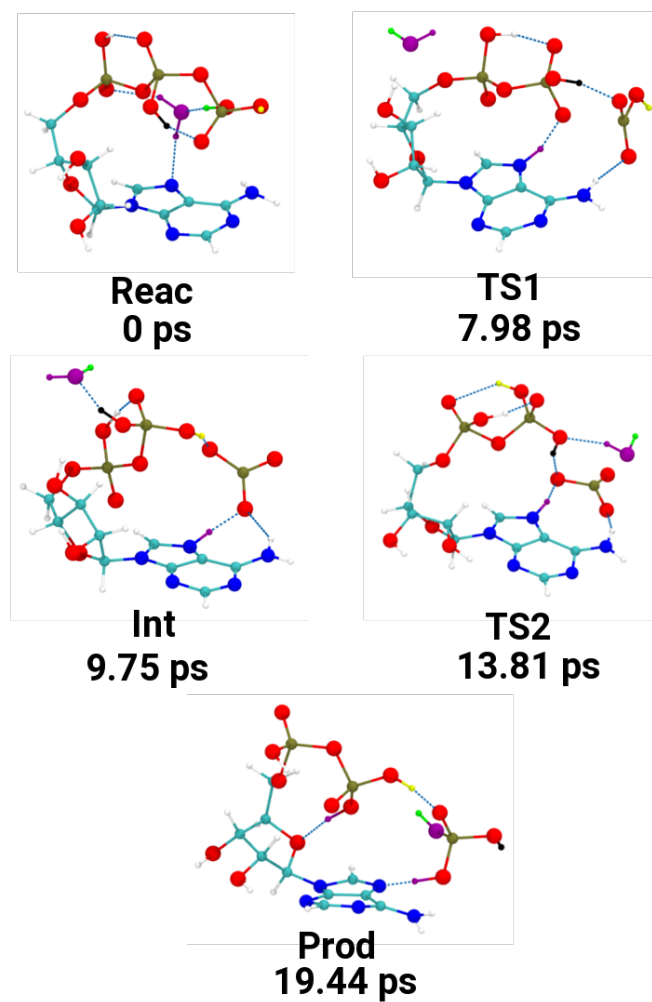


FIG. 4. Snapshots of H-ATP hydrolysis in the gas-phase. See Figure 2a for approximate location of these snapshots in the free energy surface. Hydrogens are shown in white, oxygens in red, nitrogens in blue, carbons in cyan and phosphorous in tan. For clarity, the starting configuration of water molecule is shown in purple and the participating hydrogens in the reaction with different colors (green, black and yellow). Hydrogen bonds are also shown using dashed blue lines.

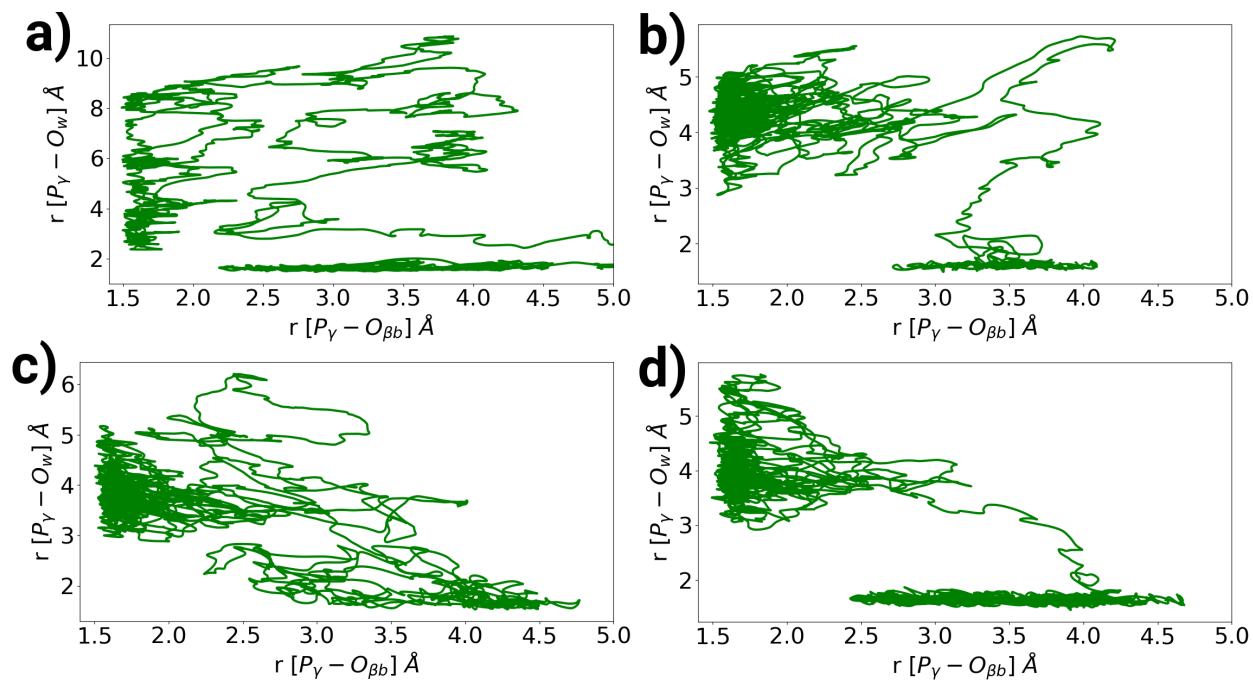


FIG. 5. More O'Ferrall-Jencks plot for the hydrolysis of a) H-ATP in the gas-phase, b) H-ATP in the aqueous-phase, c) Mg-ATP in the aqueous-phase, and d) Ca-ATP in the aqueous-phase.

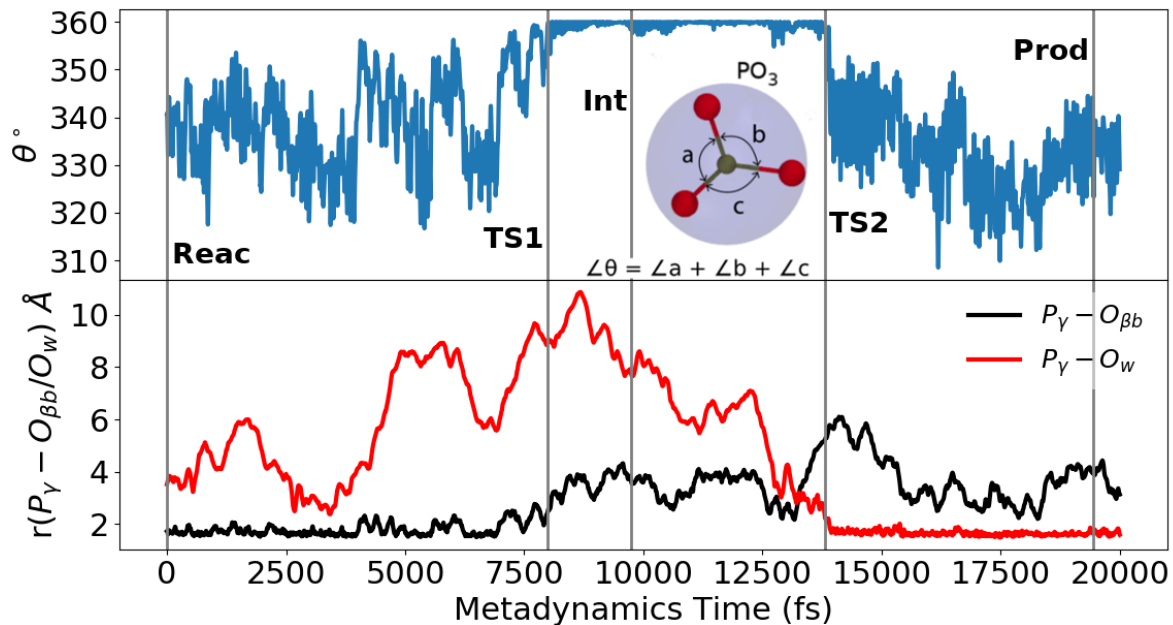


FIG. 6. **Upper panel:** Changes in  $\angle\theta$  during a metadynamics run for gas-phase hydrolysis of H-ATP. **Lower panel:** Changes in distances during a metadynamics run between  $P_\gamma$  and selected oxygen atoms for gas-phase hydrolysis of H-ATP. Phosphorus is shown in tan and oxygens in red. The symbols 'Reac', 'Int', 'Prod', 'TS1' and 'TS2' are defined in Figure 2a.

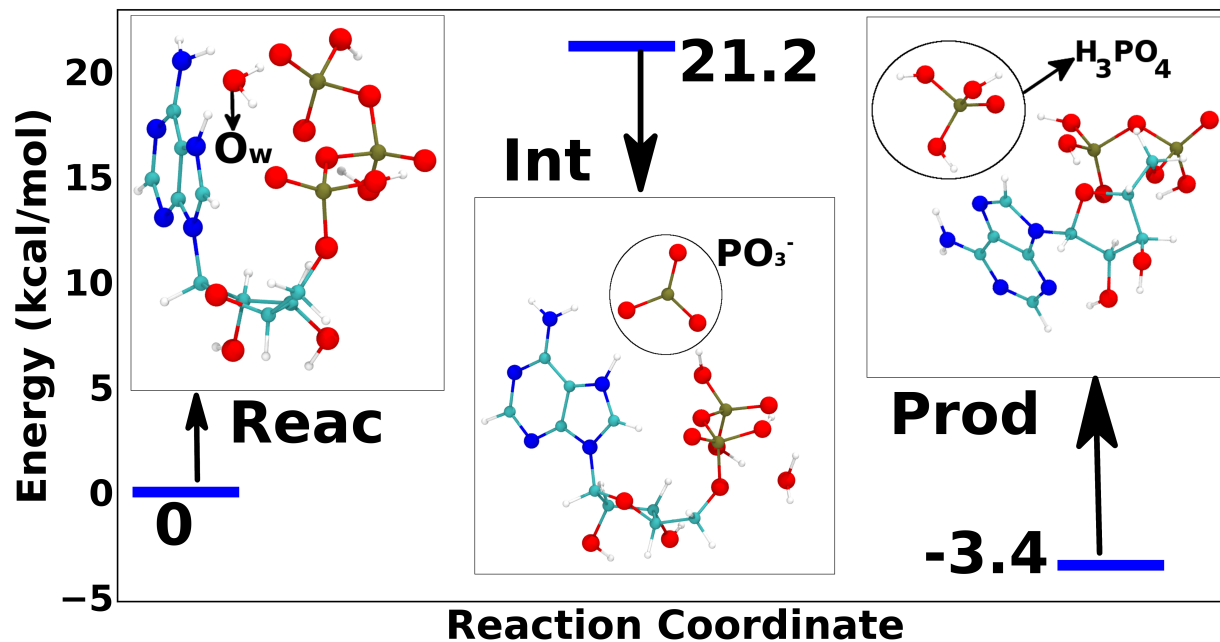


FIG. 7. Energy profile for gas-phase ATP hydrolysis. The reactant complex is taken as the zero of energy. Also shown are optimized geometries of gas-phase reactant (Reac), intermediate (Int) and product (Prod) states. Hydrogens are shown in white, oxygens in red, nitrogens in blue, carbons in cyan and phosphorous in tan. The symbols ‘Reac’, ‘Int’, and ‘Prod’ are defined in Figure 2a.

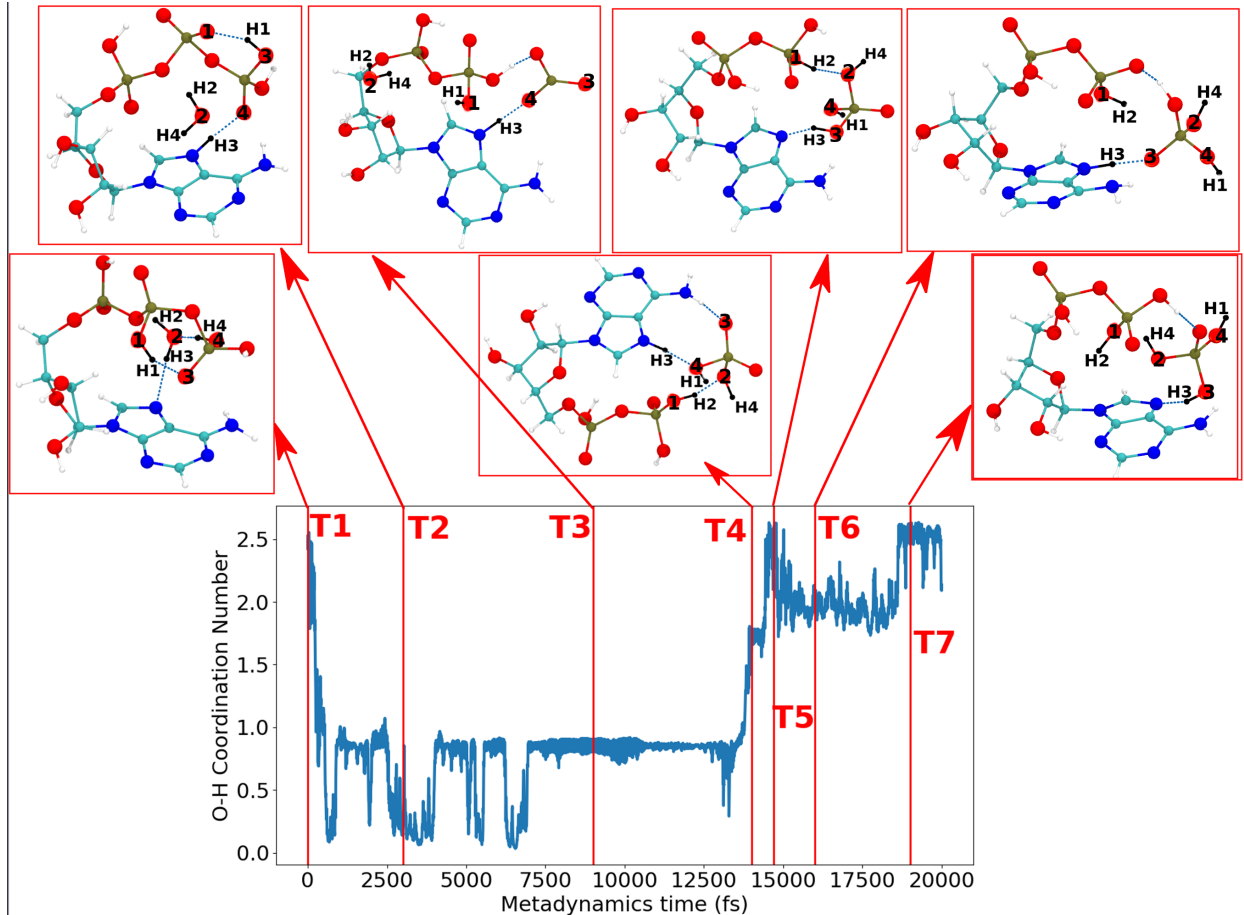


FIG. 8. Plot of O-H coordination number *vs* Metadynamics time. We also show snapshots of the complex at various times during the simulation. The O-H coordination is the sum of the coordination numbers:  $CN(O1;\{H1, H2\}) + CN(O4;\{H4, H1\}) + CN(O2;H3) + CN(O3;H3)$ .  $CN[O - H] = \sum_{j \in H} \frac{1 - (R_{OH_j}/R_{OH}^0)^6}{1 - (R_{OH_j}/R_{OH}^0)^{12}}$ . The relevant oxygens and hydrogens are numbered in the snapshots.

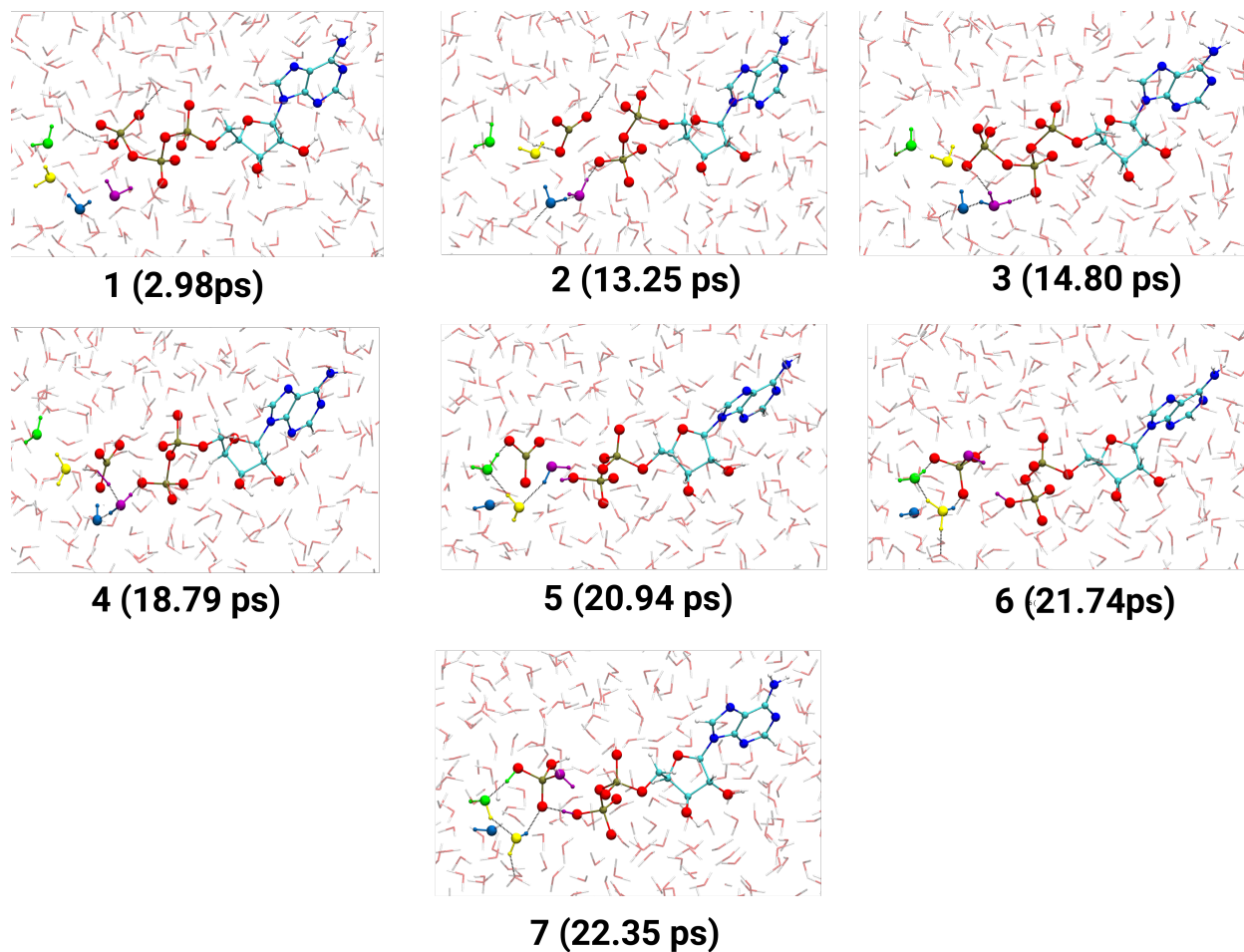


FIG. 9. Snapshots of H-ATP hydrolysis in aqueous solution during a metadynamics run. We use the following color coding to depict atoms: Hydrogens in white, Oxygens in red, Nitrogens in blue, Carbons in cyan, and Phosphorus in tan. Lytic water molecule finally attacking the metaphosphate is shown in purple and the assisting water molecules are shown in blue, yellow and green. For clarity, all the other water molecules are blurred. Some hydrogen bonds are also shown using dashed black lines.

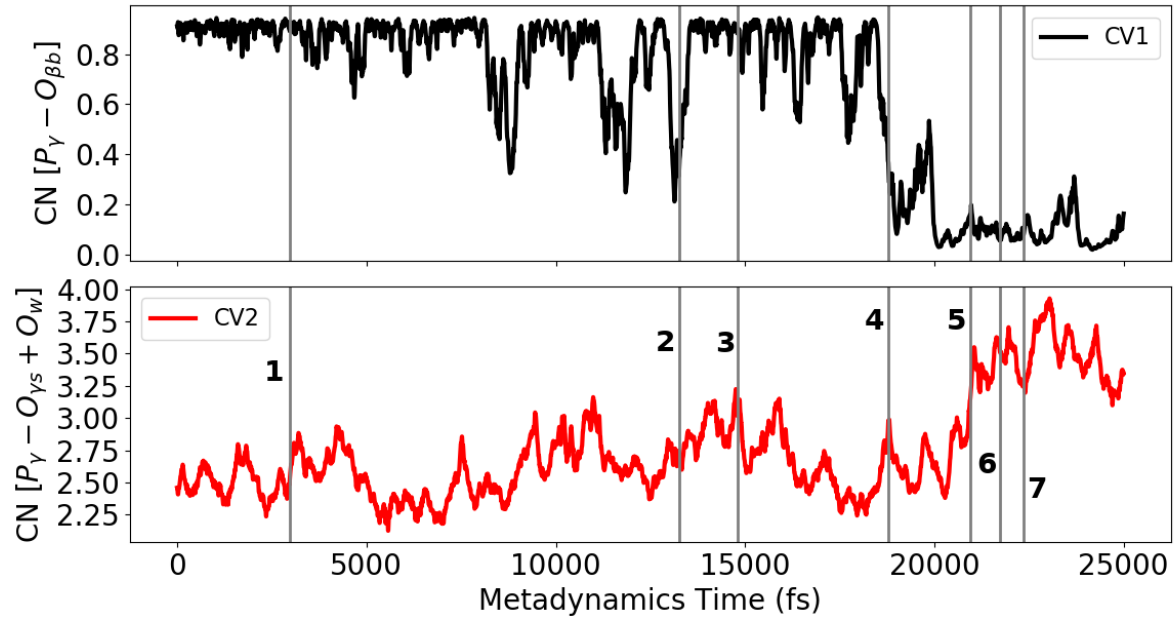


FIG. 10. Evolution of collective variables during hydrolysis of H-ATP in the aqueous solution. See Sec. IIB2 for definitions of CV1 and CV2. The snapshots for the numbered times are shown in Figure 9.

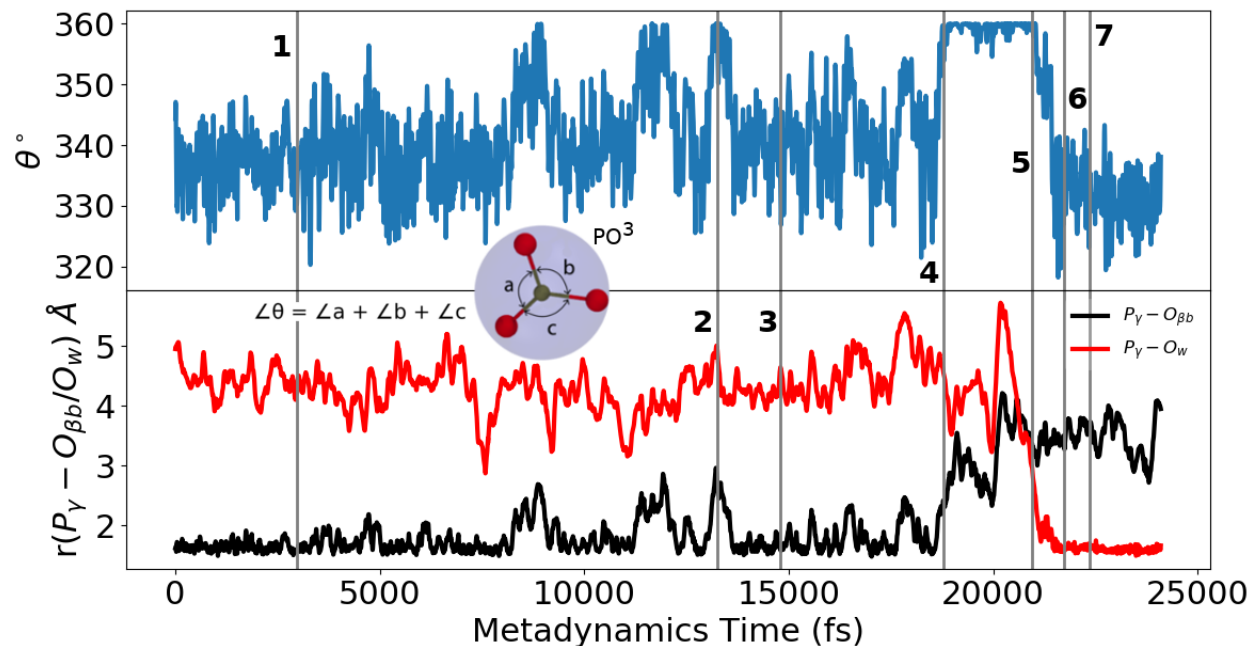


FIG. 11. **Upper panel:** Changes in  $\angle\theta$  during a metadynamics run for aqueous-phase hydrolysis of H-ATP. **Lower panel:** Changes in distances during a metadynamics run between  $P_\gamma$  and selected oxygen atoms for aqueous-phase hydrolysis of H-ATP. Phosphorus is shown in tan and oxygens in red. The snapshots for the numbered times are shown in Figure 9.

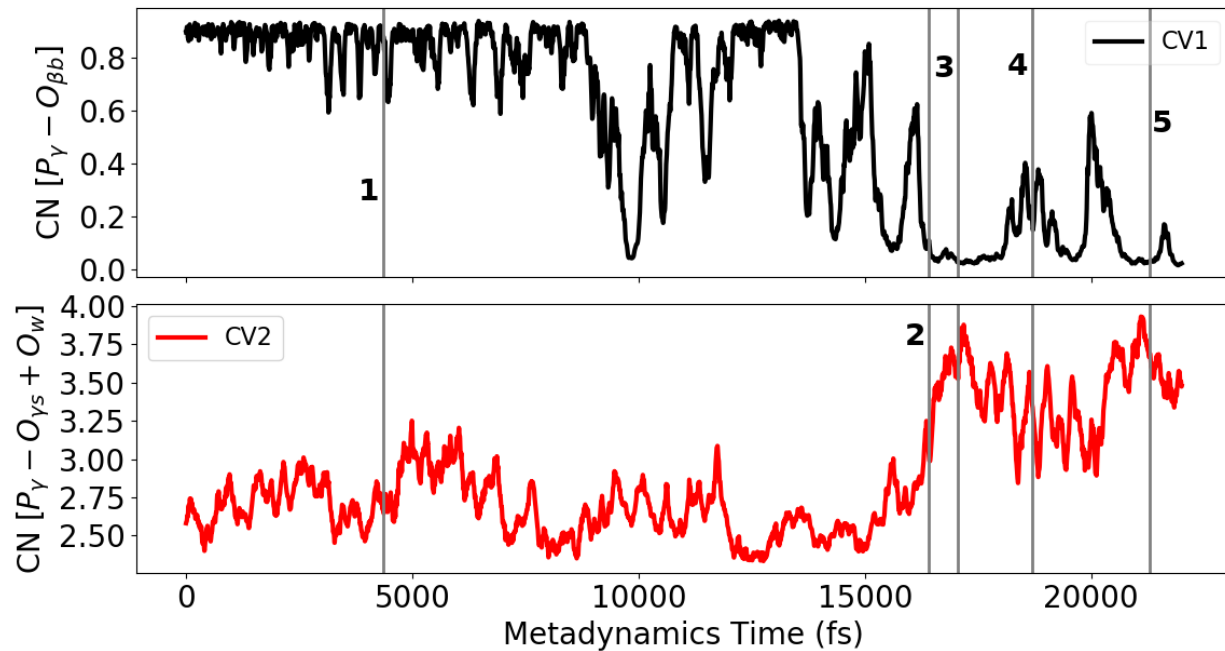


FIG. 12. Evolution of collective variables during hydrolysis of Mg-ATP in the aqueous solution. See Sec. IIB 2 for definitions of CV1 and CV2. The snapshots for the numbered times are shown in Figure 13.

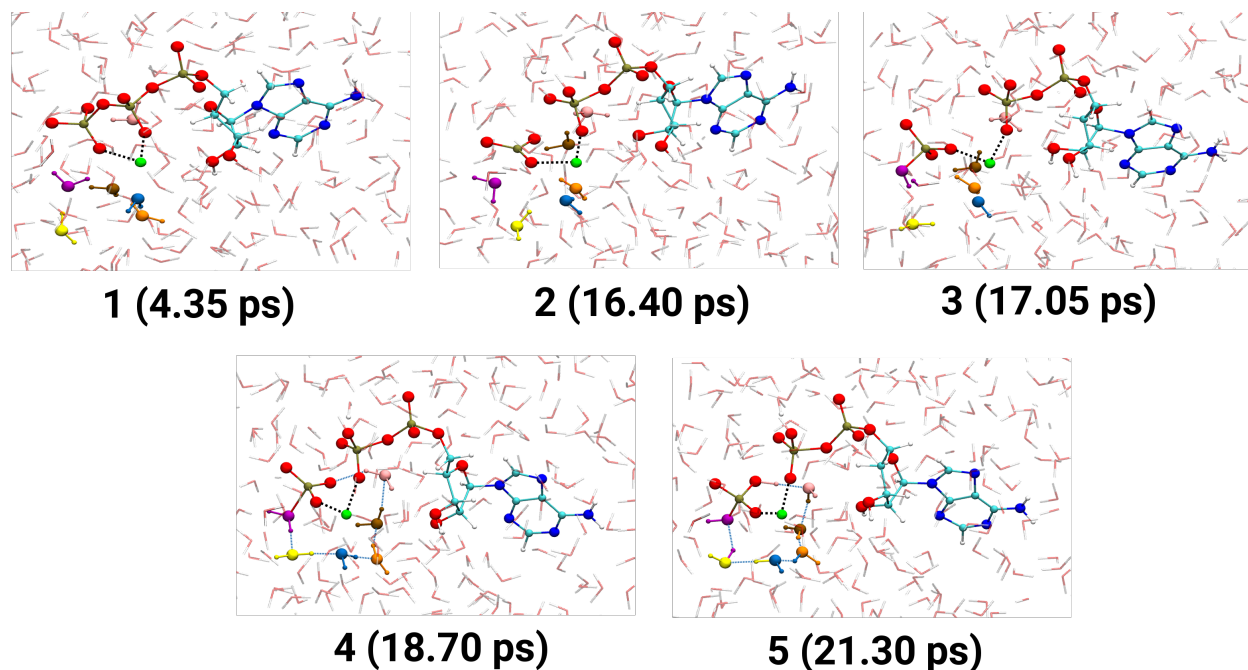


FIG. 13. Snapshots of Mg-ATP hydrolysis in aqueous solution during a metadynamics run. We use the following color coding to depict atoms: magnesium in green, hydrogens in white, oxygens in red, nitrogens in blue, carbons in cyan, and phosphorus in tan. Lytic water molecule finally attacking the metaphosphate is shown in purple and the assisting water molecules are shown in yellow, blue, orange, brown, and pink. For clarity, all the other water molecules are blurred. Some hydrogen bonds are also shown using dashed blue lines.

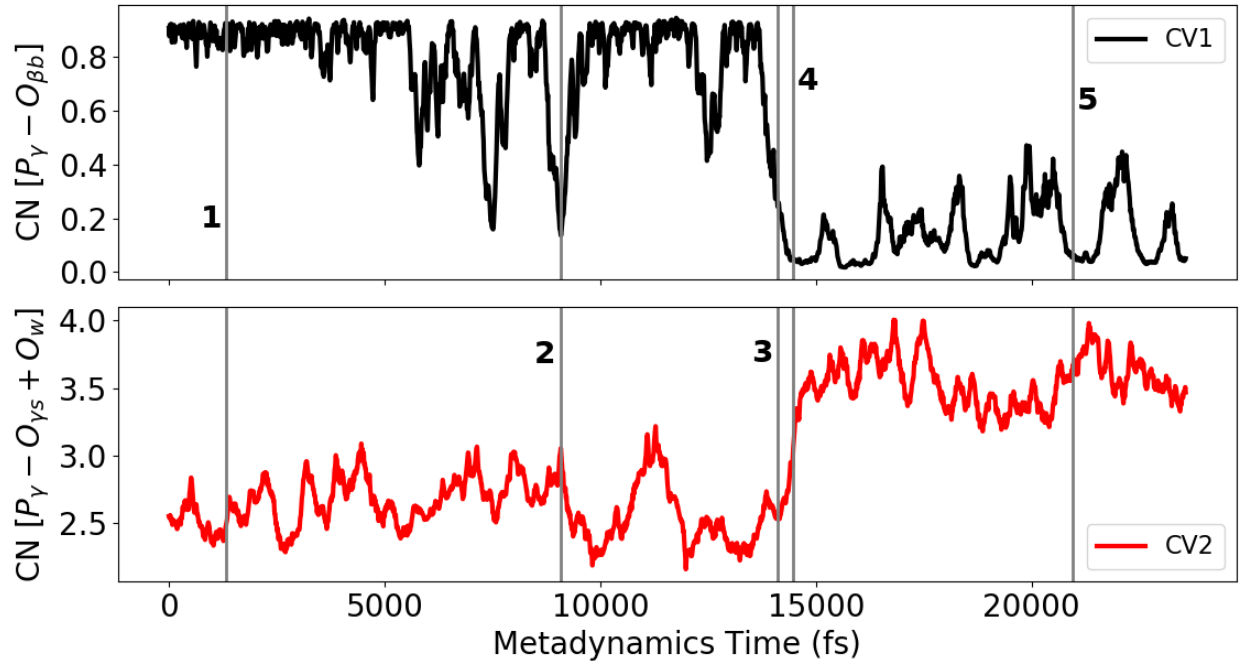


FIG. 14. Evolution of collective variables during hydrolysis of Ca-ATP in the aqueous solution. See Sec. IIB 2 for definitions of CV1 and CV2. The snapshots for the numbered times are shown in Figure 15.

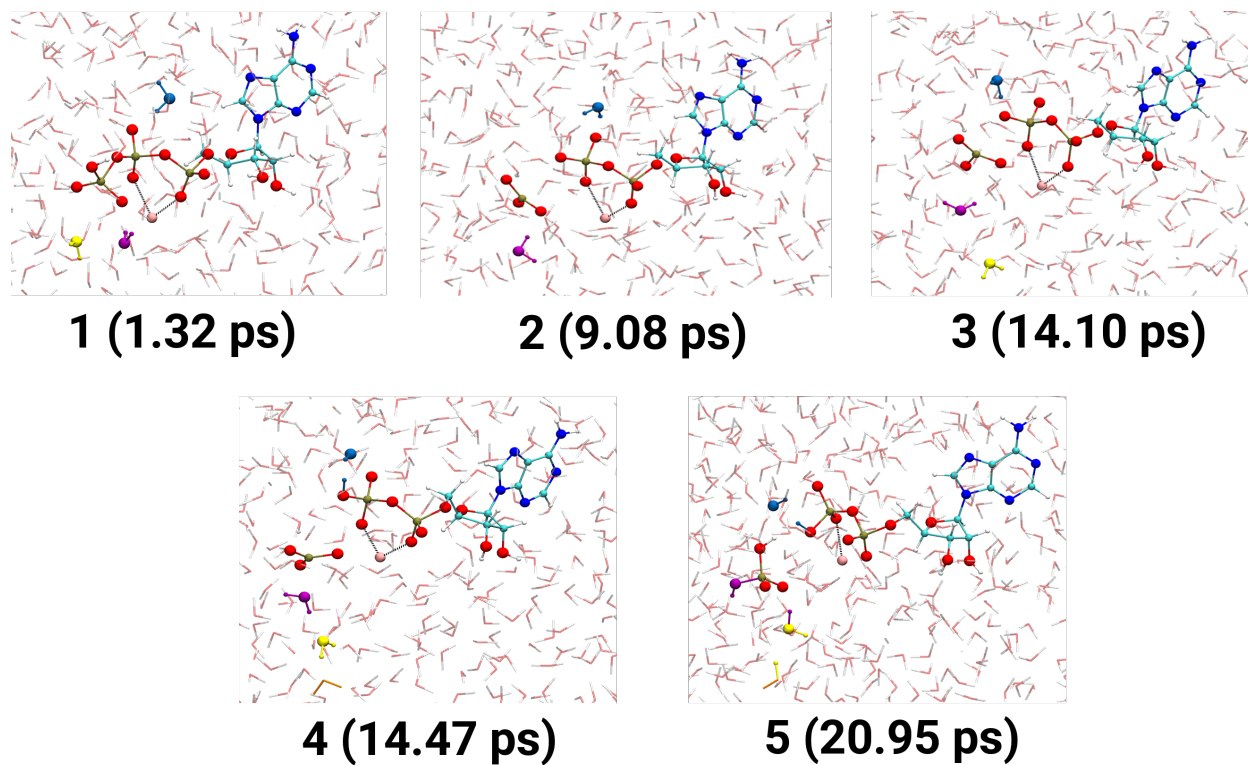


FIG. 15. Snapshots of Ca-ATP hydrolysis in aqueous solution during a metadynamics run. We use the following color coding to depict atoms: calcium in pink, hydrogens in white, oxygens in red, nitrogens in blue, carbons in cyan, and phosphorus in tan. Lytic water molecule finally attacking the metaphosphate is shown in purple and the assisting water molecules are shown in yellow and blue. For clarity, all the other water molecules are blurred.